ORIGINAL ARTICLE

Heat Shock Protein 70 as a Sex-Skewed Regulator of α-Synucleinopathy

Tarun N. Bhatia[1] · Rachel N. Clark[1] · Patrick G. Needham[2] · Kristin M. Miner[1] · Anuj S. Jamenis[1] ·
Elizabeth A. Eckhoff[1] · Nevil Abraham[1] · Xiaoming Hu[3] · Peter Wipf[4] · Kelvin C. Luk[5] · Jeffrey L. Brodsky[2] ·
Rehana K. Leak[1]

Abstract

The role of molecular chaperones, such as heat shock protein 70 (Hsp70), is not typically studied as a function of biological sex, but by addressing this gap we might improve our understanding of proteinopathic disorders that predominate in one sex. Therefore, we exposed male or female primary hippocampal cultures to preformed α-synuclein fibrils in a model of early-stage Lewy pathology. We first discovered that two mechanistically distinct inhibitors of Hsp70 function increased phospho-α-synuclein[+] inclusions more robustly in male-derived neurons. Because Hsp70 is released into extracellular compartments and may restrict cell-to-cell transmission/amplification of α-synucleinopathy, we then tested the effects of low-endotoxin, exogenous Hsp70 (eHsp70) in primary hippocampal cultures. eHsp70 was taken up by and reduced α-synuclein[+] inclusions in cells of both sexes, but pharmacological suppression of Hsp70 function attenuated the inhibitory effect of eHsp70 on perinuclear inclusions only in male neurons. In 20-month-old male mice infused with α-synuclein fibrils in the olfactory bulb, daily intranasal eHsp70 delivery also reduced inclusion numbers and the time to locate buried food. eHsp70 penetrated the limbic system and spinal cord of male mice within 3 h but was cleared within 72 h. Unexpectedly, no evidence of eHsp70 uptake from nose into brain was observed in females. A trend towards higher expression of inducible Hsp70—but not constitutive Hsp70 or Hsp40—was observed in amygdala tissues from male subjects with Lewy body disorders compared to unaffected male controls, supporting the importance of this chaperone in human disease. Women expressed higher amygdalar Hsp70 levels compared to men, regardless of disease status. Together, these data provide a new link between biological sex and a key chaperone that orchestrates proteostasis.

Keywords Intranasal · Dementia with Lewy bodies · Parkinson's disease · Synuclein · Chaperone · Proteostasis

Introduction

Emerging evidence supports the concept that Lewy body disorders are partly proteinopathic in origin, with progressive deposition of insoluble inclusions (Lewy bodies and Lewy neurites) across the central and peripheral nervous systems [1–3]. One component of these inclusions is the abundant protein α-synuclein, which can assemble into oligomers, protofibrils, and fibrils when protein quality control collapses [4, 5]. In Lewy body disorders, these pathological forms of α-synuclein are hypothesized to spread across cells in prion-like fashion, seeding progressively more Lewy pathology in vulnerable brain regions [6–10]. Thus, by interfering with the assembly, intercellular spread, and/or amplification of toxic forms of α-synuclein, or by increasing α-synuclein degradation, new therapeutic strategies might be realized, but this type of intervention has proven difficult to achieve in the clinic.

The heat shock protein 70 (Hsp70) chaperone is highly conserved across diverse species and is one of the earliest and most dominantly expressed proteins after exposure to conditions that denature cellular proteins and trigger loss of protein homeostasis (proteostasis) [11–13]. Hsp70 facilitates

✉ Rehana K. Leak
leakr@duq.edu

1 Graduate School of Pharmaceutical Sciences, Duquesne University, Pittsburgh, PA, USA

2 Dept. of Biological Sciences, University of Pittsburgh, Pittsburgh, PA, USA

3 Dept. of Neurology, University of Pittsburgh, Pittsburgh, PA, USA

4 Dept. of Chemistry, University of Pittsburgh, Pittsburgh, PA, USA

5 Dept. of Pathology and Laboratory Medicine, University of Pennsylvania, Philadelphia, PA, USA

protein folding and the targeted degradation of misfolded proteins [14], has anti-apoptotic properties [15], blocks α-synuclein oligomerization [16], and inhibits α-synuclein fibril assembly and amyloid aggregation [17–25]. However, in Lewy body disorders, Hsp70 and its cochaperone, Hsp40, may also reside within inclusions, suggestive of possible entrapment and, therefore, cytosolic depletion [26]. Furthermore, aggregates of proteins that are implicated in the etiology of neurodegenerative disorders (such as α-synuclein) might be unable to trigger the appropriate heat shock response [27]. Thus, boosting Hsp70 levels and/or activities is expected to delay the onset and slow the progression of Lewy body disorders.

Established risk factors for the onset of Lewy body disorders include advanced age and the male sex [28, 29]. However, studies of sex differences in the progression (rather than onset) of Lewy body disorders are complicated by sex-biased baseline traits (e.g., anxiety and depression) and by lack of statistical comparisons to control subjects or drug-naïve, early-stage patients [30]. Furthermore, clinical studies often fail to stratify subjects based on differences in the topographical extent of Lewy pathology, as the latter are established postmortem. For these and other reasons, conflicting reports on sex differences are unsurprising. For example, a recent report did not reveal robust sex differences in the progression of Parkinson's disease, but female patients displayed worse patient-reported disabilities, and greater anxiety, somatization, and depression-related symptoms [31]. Higher mortality was also observed in female patients compared to males diagnosed with Parkinson's disease dementia (PDD) or dementia with Lewy bodies (DLB) [32–34]. However, in drug-naïve female Parkinson's patients, there was evidence of a 3.6-year shift to older age of onset, 38% slower deterioration, and 16% higher dopamine-transporter binding compared to male counterparts [35]. Moreover, a recent report on de novo Parkinson's disease patients concluded that, after matching for disease duration and severity, male patients demonstrated greater brain atrophy and disruptions of connectivity [36]. Another recent multicenter study on unmedicated de novo Parkinson's patients revealed worse olfaction and cognition in men and greater trait anxiety in women [37].

Despite the abovementioned clinical reports of sex differences in Lewy body disorders, few preclinical studies on the mechanisms underlying Lewy pathology have analyzed animals or cells on the basis of biological sex. In prior work [38], we observed that infusions of preformed α-synuclein fibrils in the mouse olfactory bulb/anterior olfactory nucleus (OB/AON) elicited denser inclusions in the amygdala and other select limbic regions of males compared to age-matched females. More recent studies in this preclinical model revealed greater inhibition of sucrose intake, fewer entries into an open field, and more immobile episodes in

fibril-infused male mice compared to age-matched, fibril-infused females, aside from baseline sex differences in these limbic traits (Miner et al., submitted). Although the biological mechanisms responsible for sex-biased limbic α-synucleinopathic disease are unclear, we speculate that basal or stress-induced sex differences in the limbic expression and function of factors that maintain proteostasis—such as Hsp70—might contribute. Previous studies point to higher soluble Hsp70 levels in the peripheral circulation of women [39]. Similarly, in the hypothalamus, higher Hsp70 expression was noted in female rats compared to male rats, both basally [40] and upon exposure to estradiol [41]. Higher Hsp70 expression was also reported in the female *vs.* male rat heart [42]. In contrast, *Hspa1a* and *Hspa1b* transcripts, which encode Hsp70 isoforms, may be higher in the hippocampus of male versus female mice, at least at four months of age [43]. Thus, basal or stress-induced sex differences in Hsp70 expression are likely influenced by age, but may also be tissue and/or cell-specific.

Aside from its intracellular roles, Hsp70 also functions extracellularly as an immunogenic danger signal [44–46]. Extracellular Hsp70 is found free in solution, in complexes with antigenic peptides, or associated with exosomes, and regulates innate immune responses through its "chaperokine" function [11, 47]. Extracellular Hsp70 can alternately stimulate and enter cells via receptors or the endocytic uptake of exosomes [21, 48–52]. Consequently, Hsp70 can be administered exogenously to cells and animals in recombinant form, and recent studies have therefore tested intranasal delivery of exogenous Hsp70 (eHsp70) in disease models [53–57]. Molecules delivered intranasally can penetrate the CNS via olfactory and trigeminal nerves, even as far caudally as the spinal cord, and the lipophilicity of Hsp70 may facilitate its transport from the nose into the brain [49, 50, 58–66]. Using this method, beneficial effects against experimental stroke and diabetes have been reported, and repeated intranasal eHsp70 delivery blunts cognitive dysfunction, neuron loss, and mortality in animal models of aging and Alzheimer's dementia [53–57, 67]. Two studies further reported histological and behavioral benefits of intranasal eHsp70 delivery in male rodents subjected to parkinsonism-inducing toxicants (6-hydroxydopamine and lactacystin) [68, 69]. To our knowledge, however, nose-to-brain entry of eHsp70 is untested against α-synucleinopathic disease, particularly in the limbic telencephalon. Furthermore, intranasal eHsp70 delivery has only been tested in male animals, or the sex was unmentioned [53–57, 67–69]. In sum, despite a higher disease risk in men, the impact of biological sex on the expression and function of Hsp70 in the context of Lewy body–related disease remains untested.

As a potential explanation for the sex-skewed emergence of Lewy-related pathology, we studied if male and female neuronal cells differ in their dependence on Hsp70 to

mitigate the formation of phospho-α-synuclein[+] inclusions. In addition, we tested the therapeutic potential of exogenous Hsp70 (eHsp70) in male vs. female primary hippocampal cultures challenged with α-synuclein fibrils. We also provide evidence of the entry of intranasally delivered eHsp70 into the male mouse brain, whereas no evidence of transnasal uptake was observed in female mice. In proof-of-concept studies, aged male mice were infused with intranasal eHsp70 and its impact on olfaction and inclusion formation after OB/AON α-synuclein fibril injections was tested. Finally, given the prominent olfactory/limbic pathology in Lewy body disorders [28, 70–73], we assessed olfactory bulb and amygdalar tissues harvested postmortem from men and women with Lewy body disorders and age-matched unaffected controls for the levels of Hsp70, the constitutive heat shock protein 70 (Hsc70), and the Hsp70 cochaperone, Hsp40. To our knowledge, these are the first studies to examine biological sex as an independent variable in the impact of exogenous vs. endogenous Hsp70 in the preformed fibril model of α-synucleinopathy and to test sex differences in Hsp70 expression in the olfactory bulb and amygdala of patients with Lewy body disorders.

Materials and Methods

Please see Supplemental Information (SI) for further procedural descriptions.

Primary Neuron Cultures

All procedures were performed with the approval by the Duquesne University IACUC and in accordance with the *NIH Guide for the Care and Use of Laboratory Animals*. Tissue from the hippocampus of Sprague Dawley rat brains was dissected on postnatal days 0–2. For studies in sex-divided cultures, male and female rat pups were distinguished by measuring the urethra-anus distances. To confirm the accuracy of this sexing technique, PCR for the Y-linked *Sry* gene (Mouse Genotype, Escondido, CA) was performed on their tail snips. Rat pups were bred in-house and the breeder stock was regularly replenished from Hilltop Lab Animals (Scottdale, PA) to prevent genetic drift.

In this report, primary neurons were harvested and cultured using the protocol of Volpicelli-Daley et al. (2014) [74], described in detail in SI Methods. In our postnatal cultures, neurons allowed to survive longer than 16 days in vitro (DIV16) clustered together with stretched processes and a high degree of glial proliferation. Compared to the unstressed, confluent appearance of pre-DIV16 cultures, the clustering of somata after DIV16 negatively impacted the precision of our automated image analyses and was avoided (Bhatia and Leak, unpublished).

Treatments of Primary Neuron Cultures

Wild-type mouse α-synuclein fibrils were prepared as reported [74–78] or, for data shown in Fig. S1, were obtained from StressMarq Biosciences (SPR-324B, Victoria, Canada). For Fig. 2 and Figs. S4 and S5, the photostable ATTO$_{647}$ dye was custom-conjugated to wild-type mouse α-synuclein fibrils (SPR-324B, StressMarq Biosciences). Irrespective of source and type, fibrils were sonicated in a waterbath (Bransonic series model M1800, Branson Ultrasonics Corporation, Danbury CT) for 60 min immediately before use, according to our established methods [38, 79, 80]. Cultures were treated with sonicated α-synuclein fibrils on DIV2 and assayed 6 h later, or on DIV5, 6, 12, or 16, as indicated in the figure legends. Details on immunocytochemical, immunoblotting, and image analyses procedures are in SI Methods. All eHsp70 and inhibitor treatments were performed in parallel with α-synuclein fibril treatment on DIV2. The Hsp70 inhibitor VER155008 was purchased from R&D Systems Inc (3803/10, Minneapolis, MN) and the Hsp70 inhibitor MAL3-101 was synthesized as described [81].

Preparation and Purification of Hsp70

Recombinant human Hsp70 protein was prepared and isolated as described [82], with endotoxin removal procedures as per manufacturer's directions (Endotoxin Removal Kit; Abcam ab239707). As a negative control in Fig. S2, a "mock" purification was carried out in parallel, in order to generate a mock transfection vehicle to control for any residual materials from the synthesis process. For the latter procedure, empty bacterial expression plasmid vector pET21a, lacking the coding sequence for Hsp70, was transformed into competent *E. coli* strain BL21(DE3) (C2527H, New England Biolabs, Ipswich, MA) and selected on Luria Broth + ampicillin plates. A single colony was picked and cells were grown to an OD$_{600}$ of 0.1 in LB + 100 μg/mL ampicillin at 37 °C. IPTG was added to the flasks to a final concentration of 0.5 mM to "induce" for 2 h at 30 °C with shaking. The cells were then harvested by centrifugation and the cell pellet was quickly frozen and stored at − 80 °C. The cell pellet was thawed and lysed by sonication in Nickel column buffer (50 mM NaPO$_4$, 300 mM NaCl, 10 mM imidazole, 5 mM mercaptoethanol), pH 7.8, plus complete protease inhibitor cocktail (Roche). The cell lysate was clarified by centrifugation and the cleared lysate was applied to a 5 mL volume Ni–NTA column (Qiagen). The column was washed with 25 mL nickel column buffer containing 30 mM imidazole and then eluted with 10 mL nickel column buffer containing 200 mM imidazole. The eluted fraction was concentrated to 2 mL in an Amicon Ultra spin column concentrator and was then subjected to overnight dialysis in 2 L of sterile PBS at 4 °C. The final dialyzed fraction was sterilized

by passing through a 0.2 μm syringe filter into a sterile 15 mL tube. Thus, this procedure replicates all the steps in the purification of human Hsp70 protein, except that the plasmid is empty vector and does not express Hsp70.

As an alternate source, we purchased recombinant human Hsp70 (< 50 EU/mg purified protein (LAL test)) from Enzo Life Sciences (ADI-ESP-555, Farmingdale, NY). For initial in vivo studies, the yeast homologue of Hsp70 (*SSA1*, ~ 74% homology with *HSPA1A*) was prepared using a published method [83] and used in Fig. 7a–h. For all in vitro and in vivo studies using denatured Hsp70, denaturation was performed immediately before use by incubating Hsp70 at 95 °C for 10 min and then plunging it in an ice bath for 10 min. This cycle was repeated twice.

Stereotaxic Surgeries

All procedures were performed with approval by the Duquesne University IACUC and in accordance with the *NIH Guide for the Care and Use of Laboratory Animals*. CD-1 mice (Charles River, Wilmington, MA) were acclimatized to a 12:12 photoperiod in the Duquesne University Animal Care Facility with ad libitum access to food and UV-disinfected water. Mice were anesthetized with 2% vaporized isoflurane, placed on a warm pad, and stabilized in a stereotaxic frame. As in our prior work [38, 79], we infused preformed WT mouse α-synuclein fibrils into the rear of the OB, which includes a horseshoe-shaped rostral bulge of the AON [84]. Waterbath-sonicated α-synuclein fibrils (5 μg in 1 μL) or an equal volume of PBS was infused into the OB/AON at a rate of 0.25 μL/min using a Hamilton syringe (80,085, Hamilton Company, Reno, NV) attached to a motorized injection pump (Stoelting, Wood Dale, IL). Infusate placement was verified by injections of blue food dye before each animal cohort was subjected to PBS/fibril injections. After a 4 min rest period, the needle was withdrawn from the burr hole. For studies on aged, 20-month-old mice (Fig. 7a–h), injections were performed at AP + 4.0 mm, ML + 1.0 mm, and DV -2.5 mm from Bregma (from top of skull rather than the dura mater). For studies on younger, 5-month-old mice (Fig. 7i–k), the DV coordinates were -3.0 mm. All stereotaxic coordinates were empirically based on practice injections of food dye in spare mice of the same age and sex, as CD-1 mice are considerably bigger than the C57 mice used for stereotaxic atlases.

Animals received 0.05 mg/kg buprenorphine s.c., immediately after the surgery, and were placed on an electric heating pad until recovery of ambulation. Topical lidocaine was applied at the incision site immediately after the surgery and for 3 days following the surgical procedure. Further details about the perfusion protocol and histological analyses are provided in SI Methods.

Intranasal Infusions

Mice were anesthetized using isoflurane and the indicated doses of eHsp70 (or an equivalent volume of PBS) were pipetted into the nares, as described in previous reports [53–57, 67]. Following placement of the eHsp70 drop, the animal remained anesthetized, in a supine position, to facilitate inhalation of the droplet and transnasal absorption into brain tissues. For the initial pilot studies in Fig. 6a–b, five male mice received PBS infusions (2 μL) and 5 male mice received intranasal eHsp70 (2 μg; Enzo), all at 3 months of age.

We repeated the above studies in 17–21-month-old male and female mice to corroborate nose-to-brain entry in aged animals and to characterize the time-dependent kinetics of eHsp70 clearance from the aged brain. For these latter experiments, 6 μg of eHsp70 (Enzo) was infused through the nostrils, based on higher concentrations used in prior reports [55]. Mice were anesthetized, decapitated, and their OB/AON, entorhinal cortices, brainstems, and cervical spinal cords were dissected at 3 h, 24 h, 48 h, and 72 h post-infusion and subjected to ultrasensitive, infrared immunoblotting. Because of promising data collected in the younger mice at 3 h post-infusion, we initially experimented on only 3 of the more expensive aged male mice in the 3 h group (Fig. 6c), to help raise the *n* of the remaining groups, but we were able to add an additional aged animal by the time data in Fig. 6d–f were generated. The spinal cords from one old male mouse belonging to the 0 h group in Fig. 6e and from one old female mouse belonging to the 72 h group in Fig. S8d were lost during brain removal and/or dissections.

Behavioral Analyses

Animals were subjected to tests for olfaction, cognition, and anxiety-related behaviors in a dimly lit arena. Videos from an overhead camera were scored by blinded observers or tracked using the AnyMaze software (Stoelting). Olfaction in Fig. 7c–d was tested by the latency to contact buried/exposed food as in our prior work [38]. In Fig. 7k, olfaction was tested by the odor habituation/dishabituation test, as described previously [85–87]. Cognitive deficits were assessed by the Y-maze test [88] and anxiety-related behaviors were tested in an open field arena [87, 89, 90]. Detailed technical descriptions, including a priori sample size and inclusion criteria, are provided in SI Methods.

Postmortem Human Samples

We acquired frozen OB and amygdalae via the NIH Neuro-BioBank (UCLA and University of Miami Brain Banks). Tissues had been harvested postmortem from men and women

clinically diagnosed with various Lewy body disorders or age-matched control subjects. The demographic information (including clinical/neuropathological diagnoses of Lewy body disorders) for all the human samples used in this study was provided to us by the brain banks and is listed in Table S3. Samples were sonicated in cell lysis buffer and subjected to standard SDS-PAGE, followed by infrared immunoblotting, as described in the SI Methods.

Statistics

Each statistical unit (i.e., the *n* per group) is presented as a colored dot in all graphs. In vitro data are presented as the mean + S.D. in bar graphs from at least 3 independent litters of rat pups, with each culture also run in duplicate or triplicate wells. Cell culture data from individual wells were averaged to yield a single value for each litter (i.e., each litter of pups formed only one *n* for the statistical analyses). In vivo data and data from clinical samples are presented as the mean + S.D. in bar graphs or the interquartile ranges in box or violin plots. Statistically significant intervariable interactions are written above respective graphs. A one-, two-, or three-way ANOVA was followed by the Bonferroni post hoc test to determine the statistical significance of main effects, interactions, and pairwise comparisons (IBM SPSS Statistics 23). Experiments on only two groups were analyzed by the Student's two-tailed, unpaired *t* test (GraphPad Prism Version 9). For heteroscedastic data in two groups, the Welch's *t* test was used. If parametric assumptions were unmet (e.g., non-Gaussian distribution), we used the two-tailed Mann–Whitney *U* (for 2 groups), or the Kruskal–Wallis (> 2 groups) (GraphPad Prism Version 9). For normally distributed data, Pearson correlation analyses were employed. For data without normal distributions, the Spearman correlation analysis was used. Alpha was set at 0.05. Wherever feasible, measurements were made by blinded observers, including all behavior and image analyses (except Western blots, as samples were loaded in a predetermined order).

Results

Characterization of Primary Neural Culture Model

For the studies reported here, we harvested cells from the rat hippocampus, as primary hippocampal neuronal cultures are a well-characterized in vitro model for preformed fibril studies [91]. Second, we observed that hippocampal cultures show higher endogenous α-synuclein expression compared to cultures from sensorimotor neocortex, entorhinal allocortex, and the OB/AON (not shown), suggestive of a greater pool of substrate available for seeding, as reported previously [91, 92]. In our experiments, α-synuclein fibril–treated primary postnatal mixed-sex hippocampal cultures did not undergo significant cell loss (Fig. S1a, d). This was confirmed by using fibrils from two independent sources (synthesized in-house at the University of Pennsylvania *vs.* manufactured at StressMarq Biosciences), at two concentrations (1 or 4 μg/mL), at two end-points (10 or 14 days post-treatment), and by two viability measures (Hoechst+ cell counts or In-Cell Western analyses for the neuron-specific marker, NeuN).

As confirmed by independent monoclonal pSer129 antibodies (mouse clone 81A from BioLegend and rabbit clone EP1536Y from Abcam), a robust increase in inclusions harboring pathologically phosphorylated α-synuclein (pSer129) was evident, regardless of fibril source, concentration, or treatment duration (Fig. S1b–c, e–f). Thus, in our hands, application of preformed fibrils models early-stage disease processes in rat neurons at 14 days of exposure (16 days after cell plating), with dense inclusion formation but no cell loss.

Some labs have observed primary neuron loss when challenged with preformed fibrils by 14 days after in vitro exposure [74, 78], whereas others reported that robust cell loss emerges on DIV21 but that inclusion density is also lessened by that time [93]. Given these collective findings, we assessed cultures 10 days after exposure to 1 μg/mL preformed fibrils (i.e., from DIV2-12) in subsequent experiments to maximize pSer129+ inclusion densities and model *early-stage* disease processes, unless noted otherwise.

Exogenous Hsp70 Reduces Inclusion Numbers in Mixed-Sex Primary Hippocampal Neuronal Cultures Challenged with Preformed α-Synuclein Fibrils

Recent literature supports the cell-to-cell spread of α-synuclein [75, 78, 94] and suggests that Hsp70 can blunt its aggregation [17–22, 25, 95]. Prior work in this area involved forced overexpression of Hsp70 and/ or α-synuclein, in vitro assessments of the biochemical effects of recombinant Hsp70 protein on aggregation of α-synuclein, or transformed cell lines. However, the impact of endogenous or exogenous Hsp70 on pSer129+ inclusions formed in situ is unclear, including in the preformed fibril model. To begin to fill these gaps, we tested if addition of eHsp70 into the extracellular medium would lessen pSer129+ α-synucleinopathy in the primary neural culture model established in Fig. S1.

Primary hippocampal cultures were treated with 1 μg/mL α-synuclein fibrils and 12.5–100 μg/mL native eHsp70 for 10 d (Fig. S2), in line with concentrations used by other groups [96]. As an additional control, mock transfection
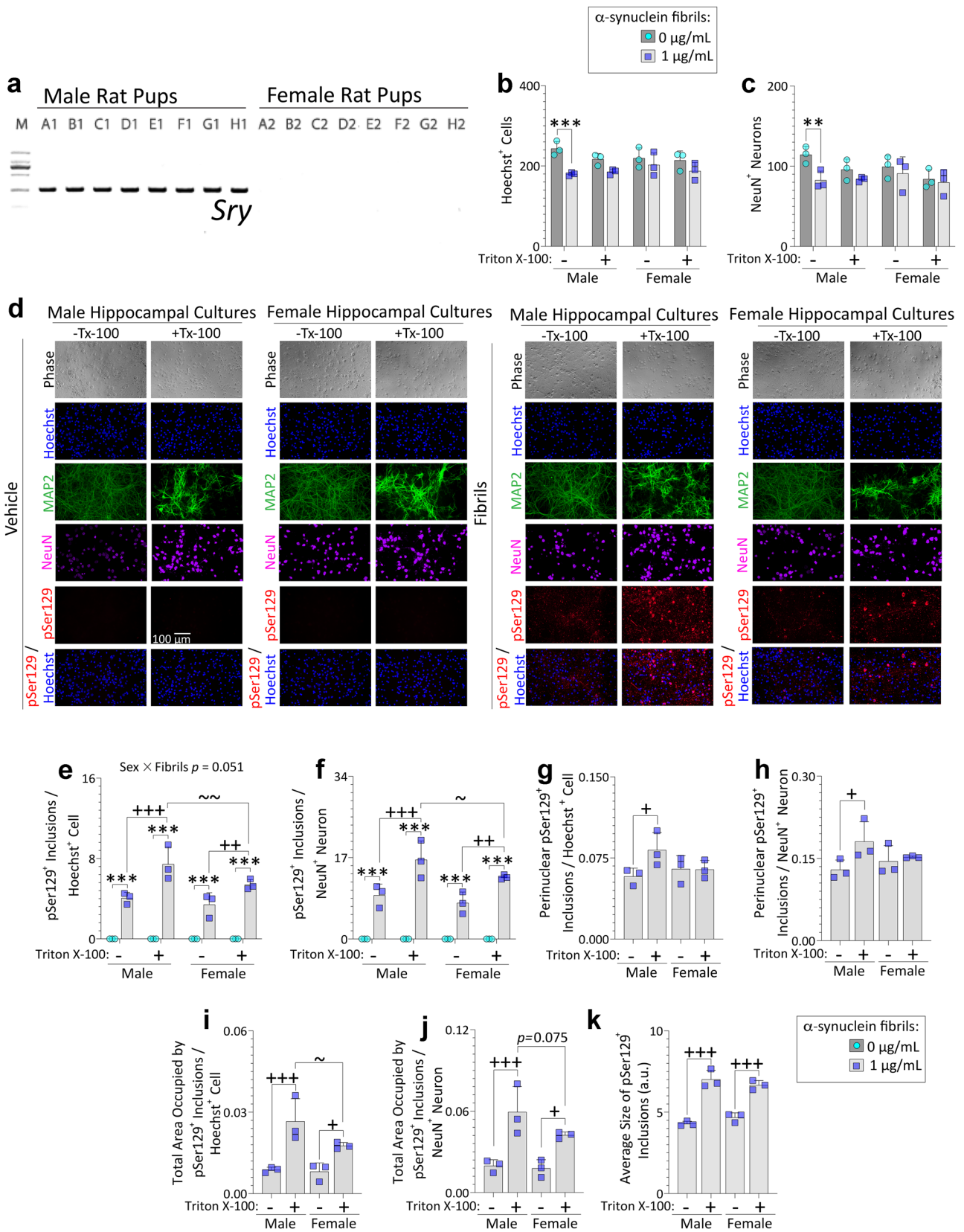
◀**Fig. 1** Male primary hippocampal cultures challenged with preformed α-synuclein fibrils develop more detergent-insoluble inclusions than female cultures. PCR for the Y-chromosome linked *Sry* gene (**a**; 273 bp) on tail snips of postnatal rat pups (see Methods). Primary hippocampal neuron cultures harvested from male *vs.* female rat pups were exposed to 1 μg/mL α-synuclein fibrils (**b–k**). After 10 days, cells were fixed with 3% formalin, with or without 1% Triton X-100. Blinded measurements of Hoechst+ cell numbers (**b**) and NeuN+ neuron numbers (**c**) are shown. Representative photomontage of phase images, pSer129+ inclusions, MAP2+ neurons, NeuN+ neurons, and Hoechst-stained nuclei in **d**. Numbers of pSer129+ inclusions, expressed as a fraction of Hoechst+ cell numbers (**e**) or NeuN+ neuron numbers (**f**). Blinded measurements of perinuclear inclusion counts expressed as a fraction of Hoechst+ cell numbers (**g**) or NeuN+ neuron numbers (**h**). Total area occupied by the inclusions expressed as a fraction of Hoechst+ cell numbers (**i**) or NeuN+ neuron numbers (**j**). The average size of the inclusions is shown in (**k**). Shown are the mean + SD of 3 independent experiments, each performed in triplicate wells. A trend toward a statistical interaction with biological sex is shown above the graph in **e**. ** $p \le 0.01$, *** $p \le 0.001$ for 0 vs. 1 μg/mL α-synuclein fibrils; $+ p \le 0.05, + + p \le 0.01, + + + p \le 0.001$ for 0 vs. 1% Triton X-100; $\sim p \le 0.05, \sim \sim p \le 0.01$ for male vs. female, two or three-way ANOVA followed by Bonferroni post hoc

vehicle (defined in Methods) was also delivered at escalating concentrations to tease apart any residual impact of the synthesis process per se. We noted that the anti-human eHsp70 antibody did not cross-react with the endogenous rodent Hsp70 via immunocytochemistry (Fig. S2a). There was a reduction in the density of pSer129+ inclusions with 100 μg/mL eHsp70 compared to the mock transfection control, an effect additionally confirmed by In-Cell Western analyses for pSer129+ α-synuclein protein (Fig. S2b–e). Although there was no statistically significant impact of eHsp70 treatment on cell viability or on inclusion size (Fig. S2d, h), 100 μg/mL eHsp70 tended to reduce the total area occupied by inclusions per cell (inclusion load) compared to the concentration-matched mock-transfection vehicle control ($p = 0.053$; Fig. S2f–g).

Using the human eHsp70 antibody employed in Fig. S2a, we observed a tendency toward absence of overlap of eHsp70 with pSer129+ inclusions; rare exceptions are noted with arrowheads in the field of view displayed in Fig. S2i–j. These observations were confirmed in subsequent experiments in sex-stratified primary hippocampal cultures, as noted below. These data suggest that exposure of primary hippocampal cultures to eHsp70 may reduce inclusion formation, increase inclusion degradation, or both.

To assess the reproducibility of our findings, we repeated the experiments with an independent source of eHsp70 (Fig. S3; Enzo's ADI-ESP-555, certified as low in endotoxins), after ensuring lack of degradation products in this preparation by immunoblotting (Fig. S3a). Primary hippocampal cultures were then exposed to vehicle or α-synuclein fibrils as well as to 75 μg/mL of the low-endotoxin eHsp70 or vehicle (also acquired from Enzo to fully control against their specific vehicle). After 10 days of treatment, cell

lysates were collected and separated by ultracentrifugation into Triton-X soluble vs. insoluble fractions, as described by Volpicelli-Daley et al. [74] (Fig. S3b–c). The pan-α-synuclein antibody displayed affinity for the positive control (preformed fibrils alone) at both low and higher molecular masses, but preformed fibrils were not similarly tagged by the pSer129 antibody, given that these are not phosphorylated, as also noted by others [74, 78].

Unexpectedly, pSer129 and pan-α-synuclein levels in the Triton-X insoluble fraction of the fibril-treated groups were not reproducibly lowered by eHsp70 treatment (Fig. S3b–c). On the other hand, eHsp70 reliably reduced the numbers of pSer129+ inclusions when assessed in situ (Fig. S3d-e). Notably, 75 μg/mL of eHsp70 halved the total area occupied by the inclusions per cell (Fig. S3d–e). These collective findings suggest that, while overall pSer129 and pan-α-synuclein levels in the Triton-X insoluble fraction are unaltered by eHsp70, the inclusion load is decreased when assessed in situ.

Primary Hippocampal Cultures Harvested from Female Rats Develop Fewer Nonionic Detergent-Insoluble pSer129+ Inclusions Than Their Male Counterparts

The aforementioned studies show that eHsp70 reduces pSer129-immunostained inclusions in mixed-sex primary cultures. To extend these findings with sex as a biological variable, male *vs.* female rat pups were distinguished based on their anogenital distances and confirmed by PCR for the Y-chromosome linked *Sry* gene (Fig. 1a). Sex-divided primary hippocampal cultures were then exposed to α-synuclein fibrils for 10 days in vitro, as justified above. As shown in Fig. 1b, fibril exposure elicited mild cell loss only in cells derived from males. Given that our postnatal neuron cultures contain some glia [97], we also performed counts of NeuN+ neurons and used this value as a second normalization standard, apart from Hoechst+ nuclei. As shown below, the former is somewhat labile in expression, but Hoechst cannot distinguish neurons from glia; hence, there are advantages to presenting both.

Consistent with the data presented above, counts of NeuN+ neurons also revealed a loss with fibril treatment only in cells from males, in agreement with counts of Hoechst+ nuclei, and the effect size was similarly modest (Fig. 1b–c). pSer129 immunostaining did not reveal baseline biological sex differences in the numbers of inclusions, unless Triton X-100 was added during fixation (Fig. 1d–f). As observed by Volpicelli-Daley et al. [98], Triton-X exposure did not solubilize the pSer129+ inclusions (Fig. 1d). Rather, an increase in inclusions was noted with addition of Triton-X during the fixation step, likely related to even greater epitope exposure, compared

to only using Triton-X post-fixation. Blinded counts of pSer129[+] inclusions (Fig. 1e–f), perinuclear pSer129[+] inclusions (Fig. 1g–h), and measurements of the total area occupied by pSer129[+] inclusions (Fig. 1i–j) suggest that male cells harbored a slightly greater load of non-ionic detergent-insoluble pSer129[+] inclusions compared to females, regardless of the normalization standard. In contrast, the average size of inclusions did not differ across sexes (Fig. 1k).

Next, we assessed whether the mild sex differences noted above might simply be associated with differential α-synuclein fibril uptake. Based on difficulties in finding a fibril-specific antibody (data not shown and see [99]), we used α-synuclein fibrils directly tagged with the photostable fluorescent dye, ATTO$_{647}$. α-synuclein fibrils appeared to colocalize with NeuN^{+} neurons more readily than with GFAP[+] astrocytes (slice views in Fig. S4a; arrows denote fewer instances of colocalization with GFAP[+] astroglia). Nuclear localization of fibrils was confirmed in Figure S4b. Z-stack analyses suggest that α-synuclein fibrils are also present in MAP2^{+} somatodendritic compartments (Fig. 2a) and β-III tubulin[+] neuritic processes (Fig. 2b). As antibodies against the axon marker tau failed our specificity tests, we leveraged β-III tubulin-positive and MAP2-negative staining of axonal processes, a subtractive technique also deployed by other groups [100, 101]. The intersection of the lines in the z-stack in Fig. 2b points to relatively rare instances of fibrils located within β-III tubulin-positive but MAP2-negative processes (further illustrated by arrows in Fig. S4c in a single slice from the same Z-stack as Fig. 2b, because the intersecting lines interfere with visualization of small structures).

We then focused our quantitative measurements on NeuN[+] "regions of interest," which are precisely recognized by the threshold feature on the cellSens software, unlike the other neuronal markers. As shown in Fig. 2c (full set of images in Fig. S5a), no differences in the uptake of α-synuclein fibrils by male vs. female NeuN[+] structures were noted, suggesting that the greater densities of nonionic detergent-insoluble inclusions in male cultures shown in Fig. 1 do not reflect sex-skewed uptake of preformed α-synuclein fibrils.

Above, we have shown uptake of α-synuclein fibrils by neuronal profiles, within 4 days of application. In order to capture potential uptake of fibrils by neuronal processes at earlier timepoints, we assessed fibril uptake at 6 h post-application (Fig. S5b–c). Even at this early time point, α-synuclein fibrils were more readily localized within somata or dendrites (Fig. S5c). Arrows in the z-stacks of Fig. S5c (same field of view as Fig. S5b but at higher MAP2 intensity scaling to confirm lack of immunopositivity) point to rare instances where fibrils are present within neuronal processes that are β-III tubulin-positive, but MAP2-negative (i.e., potential axons).

## Inhibition of Endogenous Hsp70 Function Worsens α-Synucleinopathy, Particularly in Male Cells

We have shown that the male bias in formation of Triton-X-insoluble inclusions in Fig. 1 is not simply associated with greater uptake of fibrils by male neurons in Fig. 2 and Figs. S4 and S5. Rather, the sex differences might be a consequence of skewed natural defenses against α-synuclein-related proteinopathy, perhaps including the expression level and/or function of *endogenous* Hsp70. To test this possibility, we exposed primary hippocampal cultures from male *vs.* female rat pups to α-synuclein fibrils and either the allosteric Hsp70 inhibitor MAL3-101 or active site inhibitor VER155008 (Fig. 3) [81, 102]. We found that Hoechst[+] cell numbers were slightly reduced by fibril exposure in male but not female cells (Fig. 3a–b), and treatment with MAL3-101 did not exacerbate α-synuclein fibril toxicity, which was confirmed by two viability assessments (Hoechst[+] cell counts in Fig. 3b and NeuN[+] neuron counts in Fig. 3c). Female cells exposed to MAL3-101 displayed higher numbers of Hoechst^{+} cells than their male counterparts, but the effect was modest (Fig. 3a–b). However, pSer129[+] inclusion counts (expressed as a fraction of Hoechst[+] cell counts or NeuN[+] neuron counts) were higher in male hippocampal cultures exposed to MAL3-101 (Fig. 3d–e). The total area occupied by the inclusions (but not average inclusion sizes) also increased after exposure to MAL3-101, but only in male cells (Fig. 3f–h), when expressed either as a fraction of Hoechst[+] cell counts or NeuN[+] neuron counts. In effect, female cells had failed to respond to the Hsp70 inhibitor MAL3-101 with any escalation in α-synucleinopathy.

Consistent with the MAL3-101 data, treatment with a mechanistically distinct Hsp70 activity inhibitor VER155008 also failed to amplify cell loss after exposure to α-synuclein fibrils, although VER155008 was somewhat toxic on its own in male cells (Fig. 3i–j). Furthermore, VER155008-treated male cells exposed to fibrils displayed slightly fewer numbers of NeuN^{+} neurons than their female counterparts (Fig. 3k). Exposure to VER155008 increased inclusion counts per Hoechst[+] cell (Fig. 3l), but not when normalized to NeuN[+] neuron counts (Fig. 3m). The total area occupied by the inclusions and average inclusion sizes were increased in both sexes (Fig. 3n, p), but the effects were slightly more prominent in male cells. An increase in the total area occupied by the inclusions was also evident only in male cells when expressed as a fraction of NeuN[+] neuron numbers (Fig. 3o).

Considered together with the MAL3-101 data, these collective findings suggest that male cells may be more reliant than female cells on Hsp70 functions to reduce inclusion growth. Alternatively, pharmacological inhibition of Hsp70 function may prevent the degradation and clearance

Fig. 2 Uptake of ATTO$_{647}$-conjugated α-synuclein fibrils into male (left column) and female (right column) primary hippocampal neurons. Primary hippocampal neuron cultures harvested from male *vs.* female rat pups were exposed to 0 or 1 μg/mL of ATTO$_{647}$-conjugated α-synuclein fibrils (**a–c**) for 4 d. **a** Z-stacks showing ATTO$_{647}$-conjugated α-synuclein fibrils in MAP2$^+$ neuronal somata in male and female cultures. **b** Z-stacks showing ATTO$_{647}$-conjugated α-synuclein fibrils in β-III tubulin$^+$ neurites that are also MAP2-negative. **c** Blinded assessments of numbers of ATTO$_{647}$-conjugated α-synuclein fibrils in NeuN$^+$ neurons. Shown in **c** are the mean + SD of 3 independent experiments, each performed in triplicate wells. *** $p \leq 0.001$ for 0 vs. 1 μg/mL ATTO$_{647}$-conjugated α-synuclein fibrils, two-way ANOVA followed by the Bonferroni post hoc
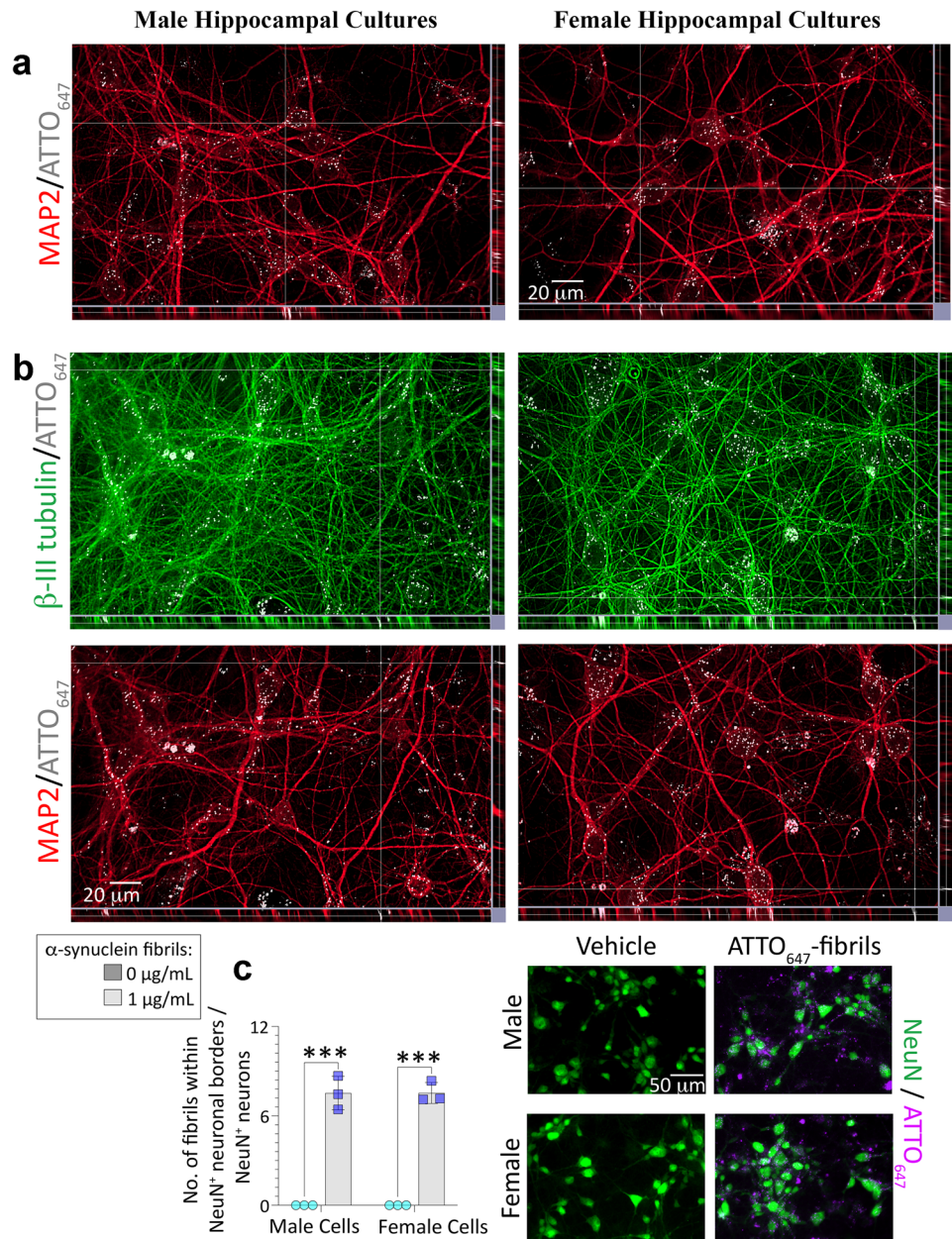

of inclusions in male neurons, thereby intensifying the α-synucleinopathy.

It is important to note that loss of Hsp70 ATPase activity with MAL3-101 or VER155008 cannot be assessed in cell or tissue extracts due to the presence of numerous other ATPases. Thus, to determine whether the sex-skewed effects might be associated with potential compensatory expression of key heat shock proteins, we performed immunoblot analyses on lysates from male *vs.* female primary hippocampal cultures treated with α-synuclein fibrils and MAL3-101 (Fig. S6). First, no changes in Hsp70 were noted (Fig. S6a–b). However, MAL3-101 and α-synuclein fibril treatment increased the levels of the constitutive form of Hsp70 (Hsc70), and the effect was female-specific

(Fig. S6c–d). MAL3-101-treated female neurons exposed to fibrils also displayed a slight increase in the levels of the Hsp70/Hsc70 co-chaperone, Hsp40 (Fig. S6e-f). Thus, the failure of MAL3-101 to increase α-synucleinopathy in female neurons in Fig. 3 may be associated with compensatory changes in Hsc70 and Hsp40 only in these cells.

eHsp70 Mitigates Inclusion Formation in Male and Female Primary Hippocampal Cultures

Based on the inhibition of Hsp70 chaperone function with MAL3-101 [20, 81, 103–106], female cells do not appear to rely on endogenous Hsp70 to the same extent as male cells. Given this sex bias, we consequently assessed sex-specific
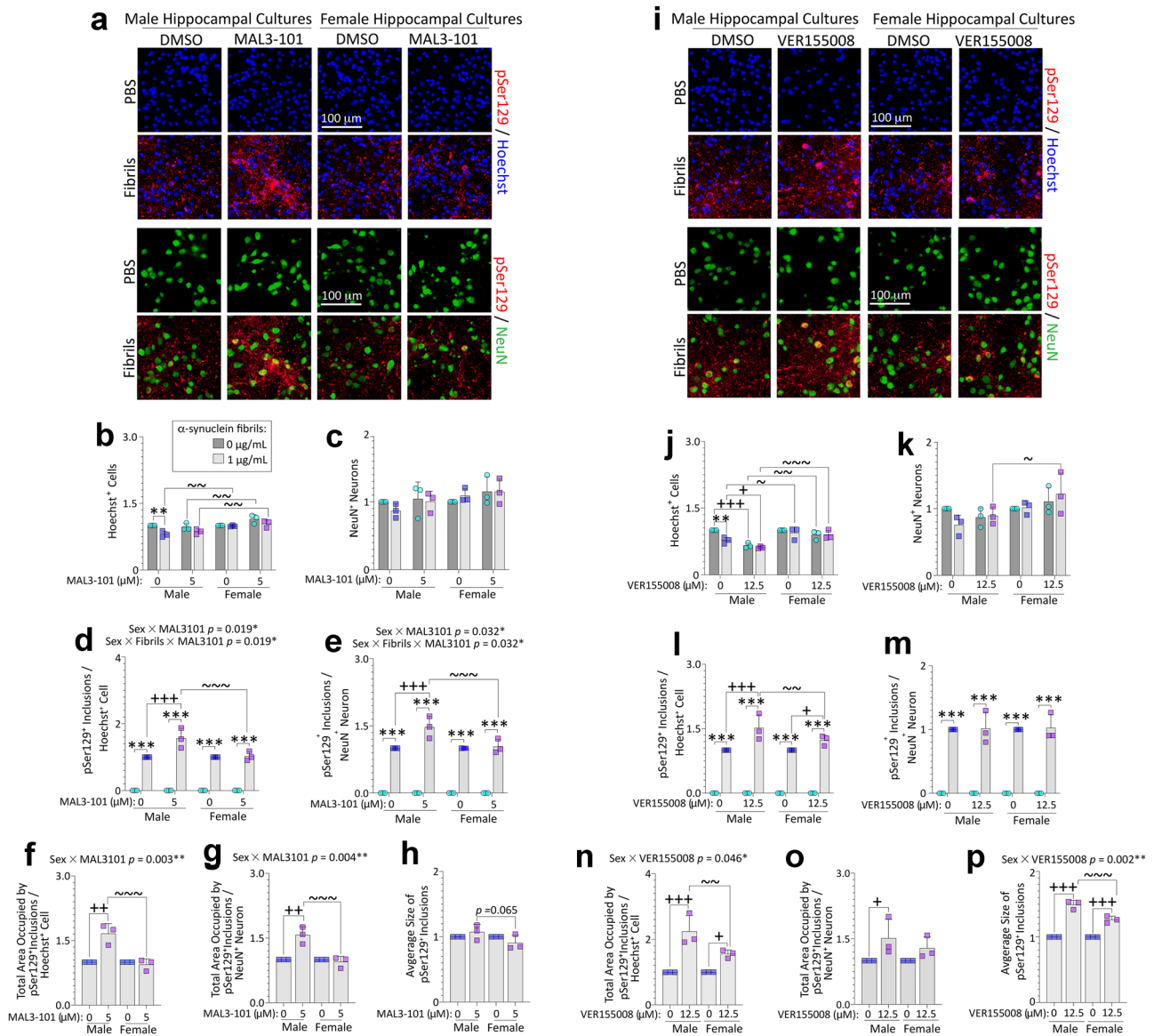
Fig. 3 Suppression of Hsp70 function with two mechanistically independent inhibitors exacerbates α-synucleinopathy in male hippocampal cultures. Primary hippocampal cultures harvested from male *vs.* female rat pups were exposed to 1 µg/mL α-synuclein fibrils for 10 days. In parallel, cells were also exposed to two independent inhibitors of endogenous Hsp70 function, MAL3-101 (5 µM; **a–h**) or VER155008 (12.5 µM; **i–p**). **a, i** Representative photomontage of pSer129+ inclusions, NeuN+ neurons, and Hoechst-stained nuclei corresponding to quantification in **b–h** or **j–p**. Quantification of numbers of Hoechst+ cells (**b, j**) and NeuN+ neurons (**c, k**). Numbers of pSer129+ inclusions expressed as a fraction of Hoechst+ cell num-

bers (**d, l**) or NeuN+ neuron numbers (**e, m**). Total area occupied by the inclusions, represented as a fraction of Hoechst+ cell numbers (**f, n**) or NeuN+ neuronal numbers (**g, o**). Average size of the inclusions is shown in **h** and **p**. Shown are the mean + SD of 3 independent experiments, each performed in triplicate wells. Significant inter-variable statistical interactions are shown above graphs in **d–g** and **n**, **p**. ** $p \leq 0.01$, *** $p \leq 0.001$ for 0 vs. 1 µg/mL α-synuclein fibrils; + $p \leq 0.05$, ++ $p \leq 0.01$, +++ $p \leq 0.001$ for vehicle vs Hsp70 inhibitor; ~ $p \leq 0.05$, ~~ $p \leq 0.01$, ~~~ $p \leq 0.001$ for male vs. female, two or three-way ANOVA followed by Bonferroni post hoc

effects of exogenous Hsp70 (eHsp70), beginning with qualitatively assessing entry of human eHsp70 protein into male and female primary hippocampal cells. First, we observed that human eHsp70 ensconced rat NeuN+ nuclei in both sexes (Fig. 4a). On occasion, eHsp70 surrounded shrunken Hoechst+ nuclei (Fig. 4b; additional examples

highlighted by arrows). In Fig. 4c, we increased brightness of the eHsp70 immunolabel to show that a majority of the eHsp70+ structures did not colocalize with pSer129+ inclusions, consistent with the findings in mixed sex cultures of Fig. S2i–j. Exceptions are noted at the intersection lines in Fig. 4c where perinuclear pSer129+ inclusions appear to be

encased by eHsp70. As expected, eHsp70 was present within β-III tubulin+ structures, close to nuclear boundaries in cells of both sexes (Fig. S7), and encapsulated some shrunken Hoechst+ nuclei (arrows in Fig. S7).

Next, we tested the importance of eHsp70 structure/function in male *vs* female cells exposed to α-synuclein fibrils (Fig. 5). In this set of experiments, we compared the impact of native eHsp70 to denatured (boiled) eHsp70, as residual materials from the manufacturing process—such as very low levels of endotoxins—would not be removed by boiling. In male cells, mild Hoechst+ cell loss was observed upon exposure to α-synuclein fibrils (Fig. 5a–b). eHsp70 did not modify the cellular toxicity of α-synuclein fibrils in male cells as per Hoechst+ cell counts (Fig. 5a–b), but the denatured form of eHsp70 appeared to reduce NeuN+ neuronal counts when administered by itself (Fig. 5c). Notably, the potential neuronal toxicity of eHsp70 was not observed in the fibril group, consistent with prior reports suggesting that intranasal delivery of eHsp70 exerts beneficial properties in murine models of Alzheimer's disease, but potentially detrimental effects in non-diseased control subjects [54, 57]. We observed some lability in NeuN expression on a per-cell basis in our cultures

(Fig. 5d), and for this reason, we continued to complement our results by measuring Hoechst+ cell numbers.

As observed with the mock transfection vehicle in Figure S2, denatured eHsp70 increased pSer129+ inclusion counts in female cells compared to PBS vehicle, but the native protein mitigated this effect (Fig. 5e–f). The average sizes of inclusions were lower in male and female cultures treated with native compared to denatured eHsp70 (Fig. 5g). In addition, native eHsp70 elicited a significant reduction in the total areas occupied by the inclusions in both male and female cultures (Fig. 5h–i), relative to its denatured form. A deeper examination of the data revealed that male cells responded less than female cells to native eHsp70 with a drop in inclusion size compared to PBS (Fig. 5g), but more robustly than female cells with a drop in inclusion counts compared to PBS (Fig. 5e). These divergent patterns may explain why total areas occupied by the inclusions do not show sex-specificity in the response to eHsp70 in Fig. 5h–i. Collectively, these data illustrate that treatment with eHsp70 may exert sex-specific effects on inclusion counts and sizes, but not on overall inclusion load or cellular uptake of eHsp70, highlighting the importance of measuring different

Fig. 4 Uptake of eHsp70 by male and female primary hippocampal cells. Primary hippocampal cultures harvested from male *vs.* female rat pups were exposed to 1 µg/mL α-synuclein fibrils and 75 µg/mL of eHsp70 for 10 days or their respective vehicles (not shown). Representative z-stack views in **a** show eHsp70 encompassing NeuN+ neuronal nuclei in both male and female cultures. Representative z-stack views in **b** show the eHsp70 within or surrounding shrunken Hoechst+ nuclei. Arrows in **b** point to additional examples outside of the point of intersection. In the z-stack images of panel **c**, eHsp70 immunolabel was brightened to show parts of perinuclear pSer129+ inclusions caged by eHsp70. Photomontages in **a–c** are all captured from the same field of view
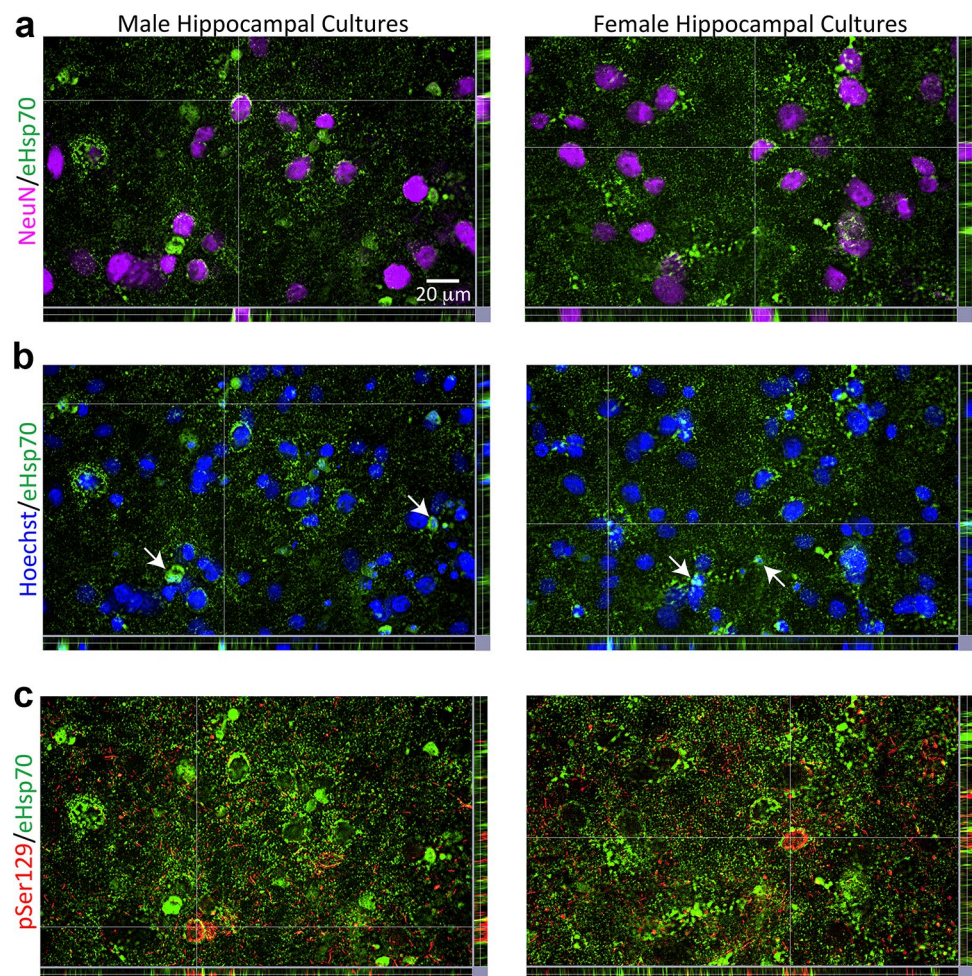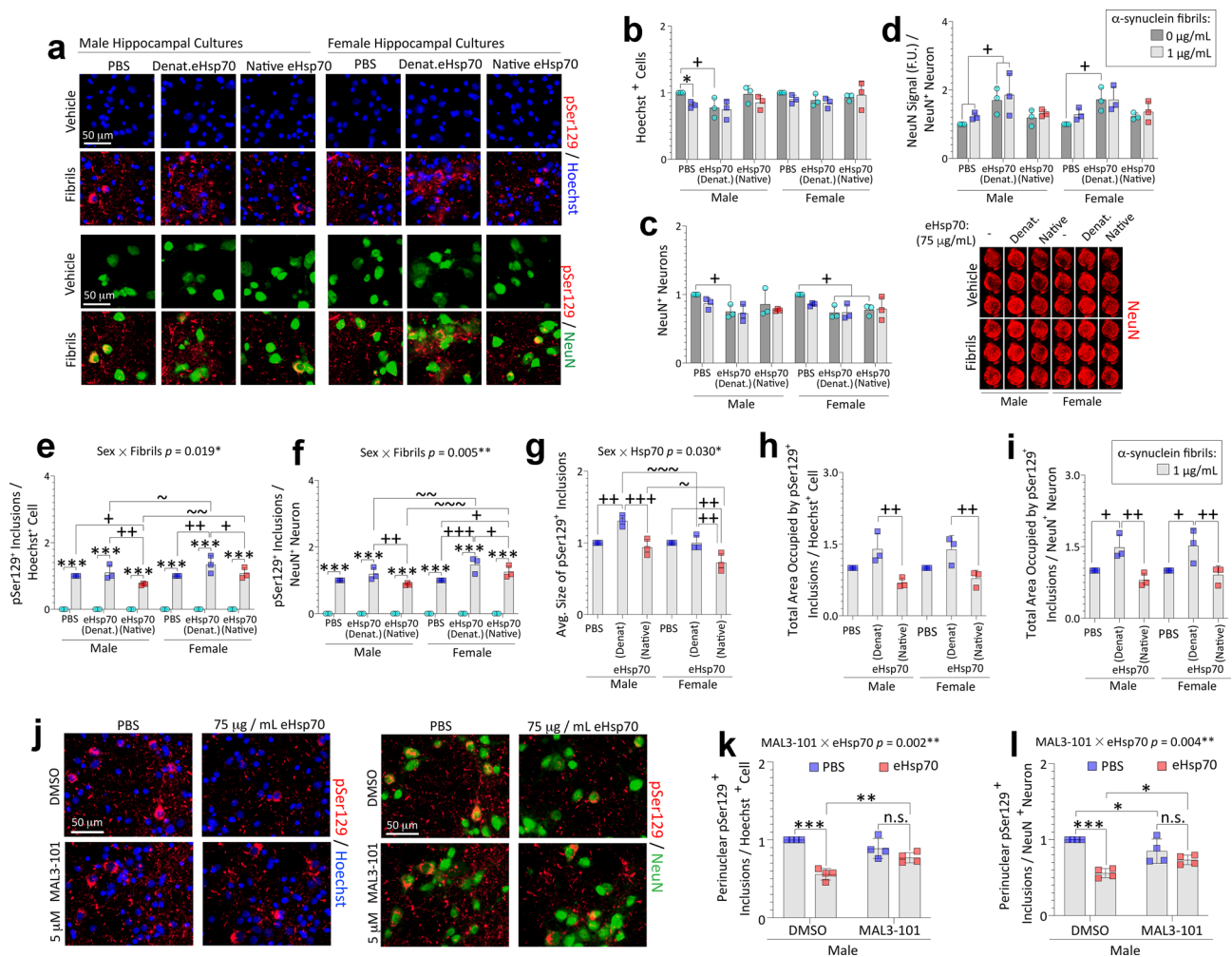
Fig. 5 Treatment with eHsp70 reduces pSer129+ inclusions in male and female primary hippocampal cultures challenged with pre-formed α-synuclein fibrils. Primary hippocampal cultures harvested from male *vs.* female rat pups were exposed to 1 µg/mL α-synuclein fibrils for 10 days. In parallel, cells were also exposed to vehicle and 75 µg/mL denatured eHsp70 (both as controls) or to 75 µg/mL of native eHsp70 (**a–i**). **a** Representative photomontage of pSer129+ inclusions, NeuN+ neurons, and Hoechst-stained nuclei corresponding to data in **b–i**. Blinded measurements of Hoechst+ cells (**b**) and NeuN+ neurons (**c**). Levels of NeuN signal (per In-Cell Western analyses) were expressed as a fraction of NeuN+ neuron counts in the same wells in **d** to display lability of the NeuN marker. Numbers of pSer129+ inclusions expressed as a fraction of Hoechst+ cells (**e**) or NeuN+ neurons (**f**). The average inclusion size is shown in **g**. The total area occupied by the inclusions expressed as a fraction of Hoechst+ cells (**h**) or NeuN+ neuron numbers (**i**). Significant inter-variable statistical interactions with biological sex are shown above

graphs in **e–g**. **j–l** Primary hippocampal neuron cultures harvested from male rat pups were exposed to 1 µg/mL α-synuclein fibrils for 10 days. In parallel, cells were also exposed to 75 µg/mL of native eHsp70 or 5 µM MAL3-101. **j** Representative photomontage of pSer129+ inclusions, NeuN+ neurons, and Hoechst-stained nuclei corresponding to data in **k–l**. Blinded measurements of numbers of perinuclear inclusions expressed as a fraction of Hoechst+ cells (**k**) or NeuN+ neuron numbers (**l**). Significant intervariable interactions above **k–l** show that MAL3-101 modifies the impact of eHsp70 on the numbers of perinuclear inclusions. Shown are the mean + SD of 3–4 independent experiments, each performed in duplicate or triplicate wells. For panels **b–i**: * $p \leq 0.05$, *** $p \leq 0.001$ for 0 vs. 1 µg/mL α-synuclein fibrils; + $p \leq 0.05$, ++ $p \leq 0.01$, +++ $p \leq 0.001$ for indicated comparison versus denatured eHsp70; ~ $p \leq 0.05$, ~~ $p \leq 0.01$, ~~~ $p \leq 0.001$ for male vs. female cells, two or three-way ANOVA followed by Bonferroni post hoc. For panels **k-l**: * $p \leq 0.05$, ** $p \leq 0.01$, *** $p \leq 0.001$, two-way ANOVA followed by Bonferroni post hoc

morphological aspects of α-synucleinopathy. Further, these findings suggest that the formation and/or degradation of inclusions is modulated by increasing the available pool of Hsp70 molecules in both male and female cells.

The Hsp70 inhibitor MAL3-101 impedes Hsp40 co-chaperone-mediated hydrolysis of ATP by Hsp70

and stimulation of Hsp70 chaperone activities [20, 81, 103–106]. To test if the beneficial effects of eHsp70 required these functions, fibril-treated primary hippocampal neuronal cultures from male rat pups were simultaneously exposed to 5 µM MAL3-101 and 75 µg/mL of native eHsp70, or to equivalent volumes of the respective
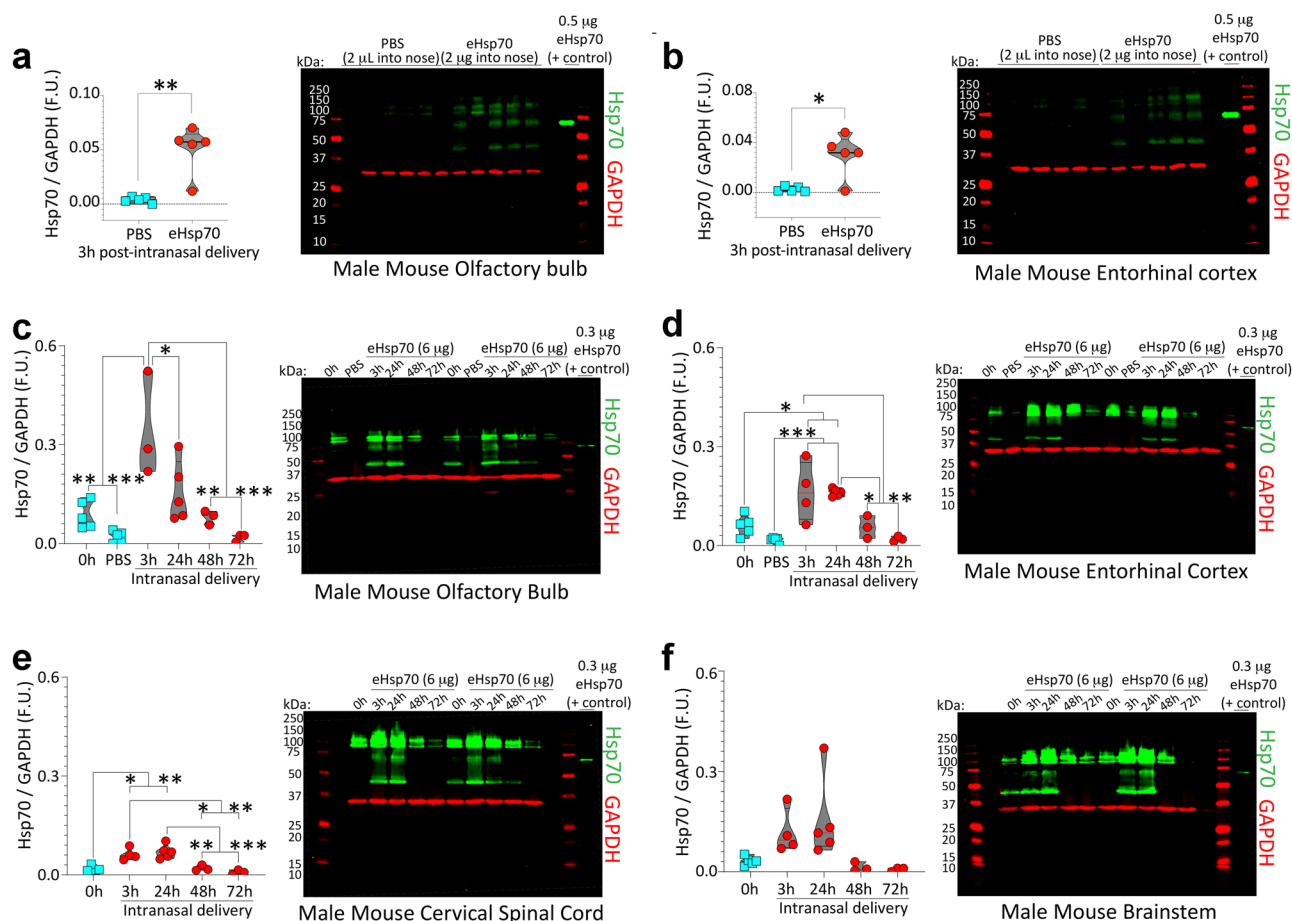
Fig. 6 eHsp70 enters the male mouse brain from the nasal cavities within 3 h and dissipates by 72 h post-infusion. **a–b** Three-month-old male mice were anesthetized with isoflurane and infused with low-endotoxin eHsp70 (2 µg; Enzo) or an equivalent volume of PBS (2 µL) behind the nares, after which the mice were left supine for 10 min and then returned to home cages. Three hours post-infusion, brains were extracted, and the olfactory bulb (**a**) and entorhinal cortices (**b**) were subjected to immunoblotting with antibodies against human Hsp70. As a positive control, recombinant human eHsp70 protein was loaded directly into the second-to-last lane of the gel. MW standards were included on both sides of all gels (red ladders). Only the band at ~70 kDa was quantified in the violin plots. Higher bands may be aggregated eHsp70 or nonspecific, and the lower bands of ~44 kDa are likely to be the cleaved ATPase domain. For studies determining eHsp70 uptake and clearance in older (17–20 months old) male

mice, 6 µg of low-endotoxin eHsp70 (Enzo) was intranasally infused and the olfactory bulb (**c**), entorhinal cortex (**d**), cervical spinal cord (**e**), and brainstem (**f**) were subjected to immunoblotting. For immunoblots in **c–f**, the positive control (recombinant eHsp70 protein) was loaded in the last lane of the gel. Brains were collected at 0 h (sham control), 3 h, 24 h, 48 h, and 72 h post-infusion. The younger PBS controls from **a–b** were also included in the blots shown in **c–d**. For the 3 h group in **c**, we began with $n = 3$ male mice but an additional n was added by the time the data in **d–f** were collected. The spinal cord from one male mouse in the 0 h group in **e** was lost during dissections. * $p \leq 0.05$, ** $p \leq 0.01$, *** $p \leq 0.001$. Data in panel **a** were analyzed by the two-tailed Mann–Whitney U. Data in panel **b** were analyzed by the two-tailed unpaired t-test with Welch's correction. Data in panels **c–f** were analyzed by the one-way ANOVA followed by Bonferroni post hoc

vehicles (Fig. 5j–l). MAL3-101 was unable to blunt the protective effects of eHsp70 on the total areas occupied by the inclusions or the numbers of pan pSer129+ inclusions (not shown). However, MAL3-101 did blunt the suppressive effect of eHsp70 on the numbers of perinuclear inclusions in male cells (Fig. 5k–l), suggesting that the perinuclear inclusions were mitigated by eHsp70 in an Hsp40-dependent manner. This finding was confirmed by using Hoechst or NeuN as the standard (Fig. 5k–l). These results and the robust statistical interactions noted above

graphs in Fig. 5k–l support the conclusion that MAL3-101 moderates the inhibitory effect of eHsp70 on perinuclear inclusion counts in male cells.

eHsp70 Enters Male Mouse Brains from the Nasal Cavities In Vivo

Intranasal delivery to the brain is noninvasive and bypasses the blood–brain barrier, intestinal degradation, and first-pass hepatic metabolism [60–64]. Prior work in other disease models
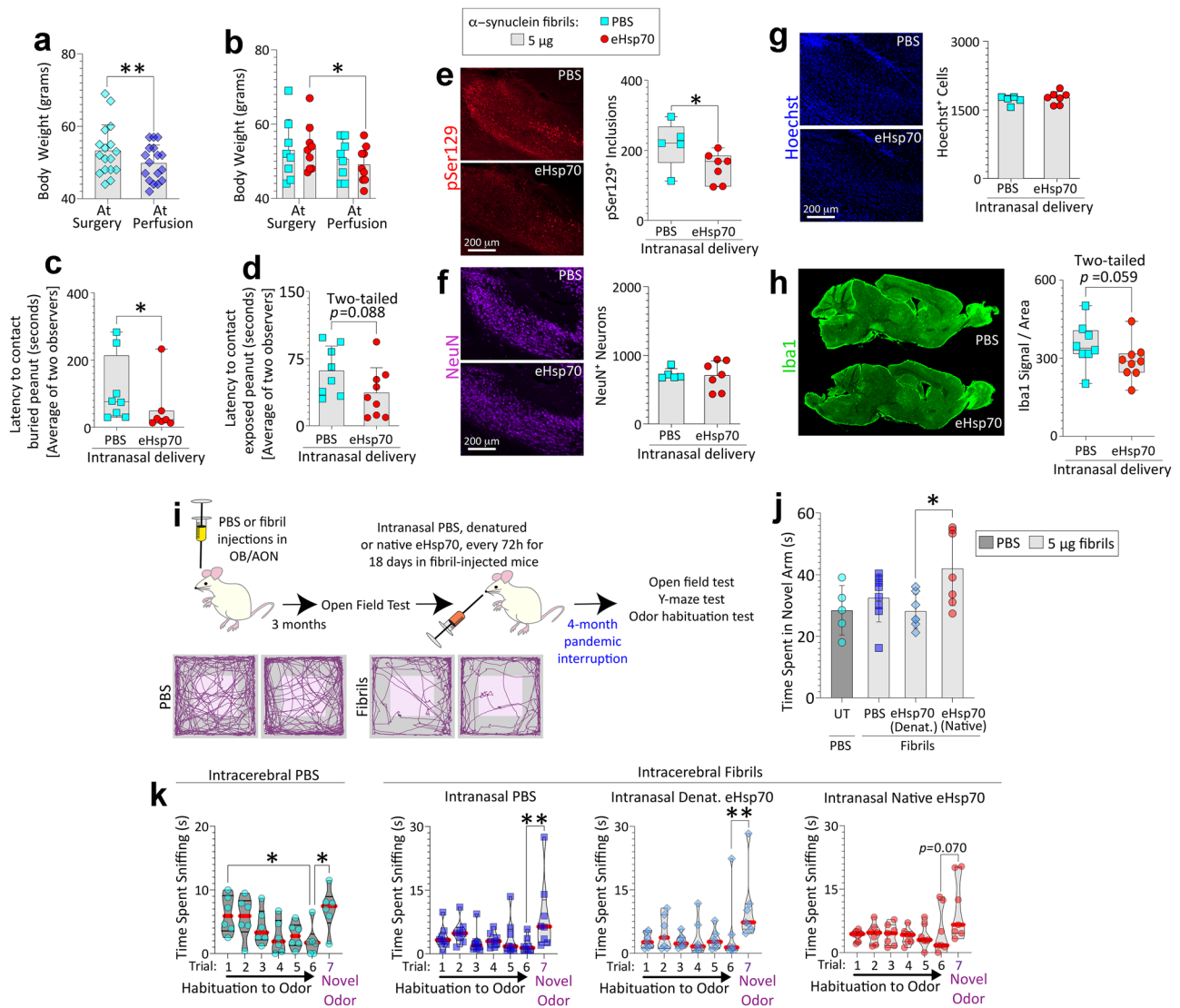
Fig. 7 Daily intranasal eHsp70 delivery for 28 days reduces inclusion numbers and the time taken to contact buried food in preformed α-synuclein fibril-injected aged male mice. Aged, 20-month-old male mice were injected with 5 µg α-synuclein fibrils in the olfactory bulb/anterior olfactory nucleus complex (OB/AON; **a–h**). After 24 h and then daily for 28 days, mice were infused with 2 µg of Ssa1 (yeast homologue of Hsp70, ~74% homology with *HSPA1A*) or an equivalent volume of sterile PBS (2 µL). See SI methods for sample sizes and exclusion criteria. Body weights are shown in **a–b**. The buried (**c**) and exposed pellet (**d**) behavior tests were performed before sacrifice and analyzed by two blinded observers (shown are the averages). Blinded measurements of pSer129[+] inclusion counts (**e**), NeuN[+] neuronal numbers (**f**), and numbers of Hoechst^{+} cells (**g**) in the AON are shown. Representative photomontages of pSer129[+] inclusions, NeuN^{+} neurons, and Hoechst-stained nuclei from the PBS or eHsp70-infused mouse AON are shown in **e–g**. Levels of Iba1 (marker for microglial activation) signal in the OB/AON were normalized by the area of the traced region in **h**. * $p \leq 0.05$, ** $p \leq 0.01$; data in panel **a** were analyzed by the two-tailed paired Student's t-test. Data in panel **b** were analyzed by the repeated measures two-way ANOVA followed by Bonferroni post hoc. Data in panels **c, e, h** were analyzed by the

two-tailed Mann–Whitney *U*. Data in panels **d, f, g** were analyzed by the two-tailed unpaired Student's t-test. **i–k** Five-month-old male mice were injected in the OB/AON with 5 µg of α-synuclein fibrils ($n=31$) or an equivalent volume of PBS (1 µL; $n=7$). See SI methods for sample sizes and exclusion criteria. Three months after fibril injections, mice were tested on an open-field apparatus to confirm behavior deficits (AnyMaze trackplots in **i**) before initiating intranasal infusions of PBS (6 µL), denatured eHsp70 (6 µg in 6 µL), or native eHsp70 (6 µg in 6 µL) to test the neurorescue potential of eHsp70 in fibril-injected mice (timeline in **i**). Due to the pandemic lockdown, we were only able to perform the intranasal infusions for 18 days, and the animals were tested on a battery of behavior tests upon our return to the lab 4 months later. Mice were tested on a Y-maze apparatus in **j** (UT = untreated). Time spent by the mice in the novel arm of the Y-maze apparatus was analyzed on AnyMaze (**j**). Data for all seven trials of the odor habituation/dishabituation test are shown in **k**. * $p \leq 0.05$, ** $p \leq 0.01$. Data in panel **j** were analyzed by one-way ANOVA followed by Bonferroni post hoc. Data in panel **k** (non-normally distributed by Shapiro–Wilk test) were analyzed by the Kruskal–Wallis test

established that intranasally delivered eHsp70 enters the rodent brain [53–57, 67–69]. Based on that work, we harvested young (3-month-old) male mouse brain tissues 3 h after intranasal infusion of 2 μg eHsp70 (Fig. 6a–b). Immunoblotting tissue extracts with antibodies against human Hsp70 suggested that eHsp70 entered the olfactory bulb (Fig. 6a) and entorhinal allocortex (Fig. 6b) within 3 h post-infusion, as expected. It is important to note that the entorhinal cortex lies at the caudal limits of the telencephalon, at a considerable distance from the nasal mucosa. Only the species representing full-length Hsp70, at ~70 kDa was quantified; immunoreactive bands at the higher molecular masses may be aggregated Hsp70 or cross-reactive species, and the lower bands are likely the cleaved ATPase domain, roughly 44 kDa in molecular mass [107, 108].

Transnasal delivery studies were then conducted in aged (17- to 21-month-old) mice of both sexes. Given the use of high eHsp70 doses by other groups [55], we chose to deliver 6 μg of eHsp70 and harvest brain tissue at 3, 24, 48, and 72 h after the single infusion. We included age-matched sham (0 h) control mice, which did not receive intranasal infusions but were anesthetized. Samples from the younger, 3-month-old, PBS-infused mice (Fig. 6a–b) were also included in Fig. 6c–d. When the intensity of the label was increased in the images (note that this had no effect on underlying quantitative data collected on the Odyssey imager), a faint species at a molecular mass of 70 kDa was visible in the aged, sham (0 h) samples, but not in the younger, PBS-infused samples, perhaps because endogenous Hsp70 expression levels can rise with age [109] and is then sufficiently high to cross-react with the anti-human Hsp70 antibody. In contrast, no cross-reaction with rodent Hsp70 by immunocytochemistry in postnatal primary neuron cultures was noted (Fig. S2a). Furthermore, immunoreactive bands at higher molecular masses were also more prominent in the samples from aged animals. Nonetheless, quantification of the blots revealed a statistically significant increase in the 70 kDa Hsp70 band in the eHsp70-infused mice. Quantitation of the immunoblots also suggested that eHsp70 penetrated the aged male olfactory bulb (Fig. 6c) along with the entorhinal cortex (Fig. 6d) and was transmitted as far caudally as the cervical spinal cord (Fig. 6e–f). Moreover, eHsp70 peaked at 3 h, lingered in the brain for up to 48 h, and dissipated within 72 h post-infusion.

Unexpectedly, there was no evidence of eHsp70 penetration into female mouse OB/AON (Fig. S8a), entorhinal cortices (Fig. S8b), brainstems (Fig. S8c), or cervical spinal cords (Fig. S8d), at the same dose and timepoints used for male mice, even though cross-reaction of the anti-human Hsp70 antibody with endogenous Hsp70 was also evident in females. These data indicate that intranasally delivered eHsp70 enters multiple parts of the central nervous system of aged male mice, and it is possible that the protein is cleared more efficiently in females and/or fails to bypass the nose-to-brain barriers (see Discussion).

Daily Intranasal Delivery of eHsp70 Following Fibril Infusions in the OB/AON Mitigates Inclusion Counts in Aged Male Mice

Prior work suggested that eHsp70 only exerts beneficial effects under pathological conditions and might be toxic under physiological conditions, as per studies in models of Alzheimer's disease [54, 57]. Thus, we limited eHsp70 delivery to fibril-infused mice to study the effects on pathological inclusions. For these studies, we leveraged a new preclinical model of olfactory-seeded Lewy body disorders, as described by us and other groups [38, 79, 110–113]. In this model, infusions of preformed fibrils in the OB elicit α-synucleinopathy along the limbic rhinencephalon as well as some deeper structures, such as the ventral tegmental area and nucleus accumbens. Inclusions form largely in neurons within weeks of infusion (see fig. 1i–j of Uemura et al. [114]). Uemura and colleagues' work further suggested that the neuronal inclusions peak in density at 1–3 months post-infusion but wane dramatically thereafter, whereas glial inclusions increase in density by 12–18 months post-infusion. In addition, loss of NeuN$^+$ structures in the AON was unexpectedly mild, as reported in aged male mice at 10.5 months post infusion by our group [38] and at 12 months post-infusion by Uemura et al. (see their fig. S1n [114]). Overall, this model seems less appropriate for examining neuroprotection against cell loss but is well suited to test therapeutic mitigation of pSer129$^+$ pathological inclusions, at early timepoints.

To this end, aged, 20-month-old male mice were injected in the OB/AON with α-synuclein fibrils and, at 24 h post-surgery, PBS or eHsp70 was delivered intranasally and daily for 28 days, based on prior work using this dosing regimen in 17-month-old mice [53]. In this initial cohort, we used a yeast Hsp70 homologue, which exhibits ~74% similarity with Hsp70 [115], and that exhibits similar properties as human Hsp70 in a range of assays [82, 103] and lacks bacterial endotoxins. Although these aged eHsp70-infused animals all lost body weight in the month post-infusion, there were no differences in weight loss between the PBS and eHsp70-infused groups (Fig. 7a–b).

Our prior work showed that male mice injected with fibrils in the OB/AON require more time to locate buried food than PBS-infused controls [38]. Here, we noted that daily eHsp70 delivery reduced the latency to contact a buried peanut in fibril-infused 21-month-old males (Fig. 7c). To assess any differences in the motivation to find food, we also tested the latency to contact an *exposed* peanut (Fig. 7d), and all mice displayed interest in the food in the latter assessment. eHsp70-infused mice showed a trend towards faster contact of the exposed peanut compared to vehicle-infused counterparts, suggestive of differences in motivation rather than olfaction alone ($p = 0.088$; Fig. 7d). In this

animal cohort, eHsp70 also reduced α-synucleinopathy in the AON (Fig. 7e). As expected, eHsp70 administration did not affect neuronal (Fig. 7f) or pan-cellular counts (Fig. 7g) upon sacrifice at 21 months of age. Further, there was a trend towards mitigation of the microglial activation marker, Iba1, upon exposure of fibril-injected aged male mice to eHsp70 ($p = 0.059$; Fig. 7h), consistent with recent work on eHsp70 in the 6-OHDA model [69].

To extend these observations and build upon the primary culture work above, we initiated an extensive, long-term in vivo study to assess the neurorescue or neurorestorative potential of human eHsp70 in fibril-injected male mice. Thus, we infused PBS, denatured eHsp70, or native eHsp70 through the nostrils after we confirmed the emergence of behavior deficits in the open-field test (~3 months following fibril infusions in the OB/AON; AnyMaze trackplots in Fig. 7i), until we were interrupted by the pandemic lockdown for 4 months. Behavior testing was only performed on this cohort of mice after our return to labs. Although there was better recognition of the novel arm in the Y-maze in the native eHsp70 group compared to the denatured eHsp70 group, this measure was unaffected by intracerebral fibril infusions per se, suggesting that the eHsp70 was not modifying any fibril-induced changes in cognition, but exerting surprisingly long-term effects on baseline cognitive function (Fig. 7j). On the other hand, no long-term change on the open-field test (not shown) or in the odor habituation/dishabituation test was noted with the transient exposure to eHsp70 (Fig. 7k). Given these negative data, brains were not assessed at the histological level.

Women Display Higher Hsp70 Levels in the Amygdala than Men

Finally, we assessed the levels of chaperones in the human limbic system by immunoblotting amygdala and olfactory bulb tissues from male and female patients diagnosed with Lewy body disorders and unaffected controls. These samples were acquired via NeuroBioBank (UCLA and University of Miami cohorts; demographics and information on diagnoses in Table S3). Age at death (Fig. 8a) and postmortem interval (Fig. 8b) of the human subjects examined in this report did not differ across groups. Whole tissue extracts were probed by immunoblotting for Hsp70 (Fig. 8), Hsp40, and Hsc70 (Figs. S9 and S10). In the olfactory bulb, no statistically significant differences in Hsp70 levels were observed across the sexes or disease states (Fig. 8c–f).

In the amygdala, there were statistically significant main effects of biological sex as well as Lewy body disorder diagnoses on Hsp70 levels (Fig. 8g–j). Further, when control and diseased samples were combined (see Fig. 8g), women expressed, on average, higher Hsp70 levels in their amygdalae than age-matched men. The impact of Lewy body disease

on Hsp70 levels in the sex-combined data did not quite reach statistical significance at the two-tailed level (two-tailed $p = 0.057$; Fig. 8h). This is because the main effect of disease on Hsp70 levels noted in Fig. 8i was largely attributable to men ($p = 0.069$), again suggestive of male reliance on Hsp70 under proteinopathic conditions. Postmortem interval was not correlated with Hsp70 expression in the olfactory bulb (two-tailed Spearman correlation; $r = -0.05301$, $p = 0.7970$) or amygdala (two-tailed Pearson correlation; $r = 0.04866$; $p = 0.8134$).

In contrast to Hsp70, no statistically significant effects of biological sex or disease state on Hsp40 or Hsc70 were observed in the olfactory bulb or amygdala (Figs. S9 and S10). Postmortem interval was not correlated with Hsp40 expression in the olfactory bulb (two-tailed Pearson correlation; $r = -0.1451$, $p = 0.4794$) or the amygdala (two-tailed Spearman correlation; $r = 0.07798$; $p = 0.7050$). Similarly, postmortem interval was not correlated with Hsc70 expression in the olfactory bulb (two-tailed Pearson correlation; $r = -0.09742$, $p = 0.6359$) or amygdala (two-tailed Spearman correlation; $r = 0.07661$; $p = 0.7099$).

In sum, the statistically significant main effect of biological sex or of Lewy body disorders on Hsp70 expression is not generalizable to these other two functionally related proteins (Hsc70 and Hsp40), supporting our focus on the functional role of Hsp70 in the sex-stratified preformed fibril model.

Discussion

According to the findings of the present study, Hsp70 may function as a sex-skewed modulator of experimental α-synucleinopathic disease (schematic in Fig. 9). In brief, we have made six sets of new observations: (1) Sex differences in α-synucleinopathy emerged when primary neurons were challenged with Hsp70 inhibitors or when nonionic detergent-soluble inclusions were removed, despite comparable capabilities of male and female neurons to take up preformed α-synuclein fibrils. These results suggest that cells isolated from male rodents exhibit greater reliance on Hsp70 function to blunt formation of inclusions (or they exhibit a decreased ability to degrade inclusions) compared to female cells, perhaps because female cells are also able to upregulate the constitutive form of Hsp70 (Hsc70) upon suppression of the inducible form. (2) Female cells harbored smaller inclusions in the presence of eHsp70, whereas in male cells eHsp70 treatment reduced the total numbers of inclusions but did not diminish inclusion size per se. This supports the importance of examining multiple aspects of α-synucleinopathy in preclinical models, including inclusion numbers, sizes, and total area occupied by the inclusions. (3) The salutary effects of eHsp70 on perinuclear inclusions

Fig. 8 Women express higher levels of Hsp70 in the amygdala than age-matched men. Olfactory bulb (OB) and amygdala tissues were obtained post-mortem from men and women with Lewy body disorders and control subjects via the NIH NeuroBioBank repository (UCLA and University of Miami cohorts) and whole-tissue extracts were subjected to immunoblotting. Age at death (**a**) and postmortem interval (**b**) across biological sexes and Lewy body disease status. Values from control and diseased subjects were combined to test the impact of biological sex on Hsp70 levels in the OB (**c**) or amygdala (**g**). Values from male and female subjects were combined to test the impact of disease on Hsp70 levels in the OB (**d**) or amygdala (**h**). The two-way ANOVA graph showing the separate impacts of sex and disease on Hsp70 levels is in **e** for the OB and in **i** for the amygdala. Full-length immunoblots are shown in **f** and **j**; the Total Protein Stain was used as the loading control. * $p \leq 0.05$; Data in **a–b** (non-normally distributed by Shapiro–Wilk test) were analyzed by the Kruskal–Wallis test. Data in **c–d** were analyzed by the two-tailed Mann–Whitney U test. Data in **e** and **i** were analyzed by the two-way ANOVA followed by the Bonferroni post hoc. Data in **g–h** were analyzed by the two-tailed unpaired Student's t-test. Statistically significant main effects are shown above the graph in **i**
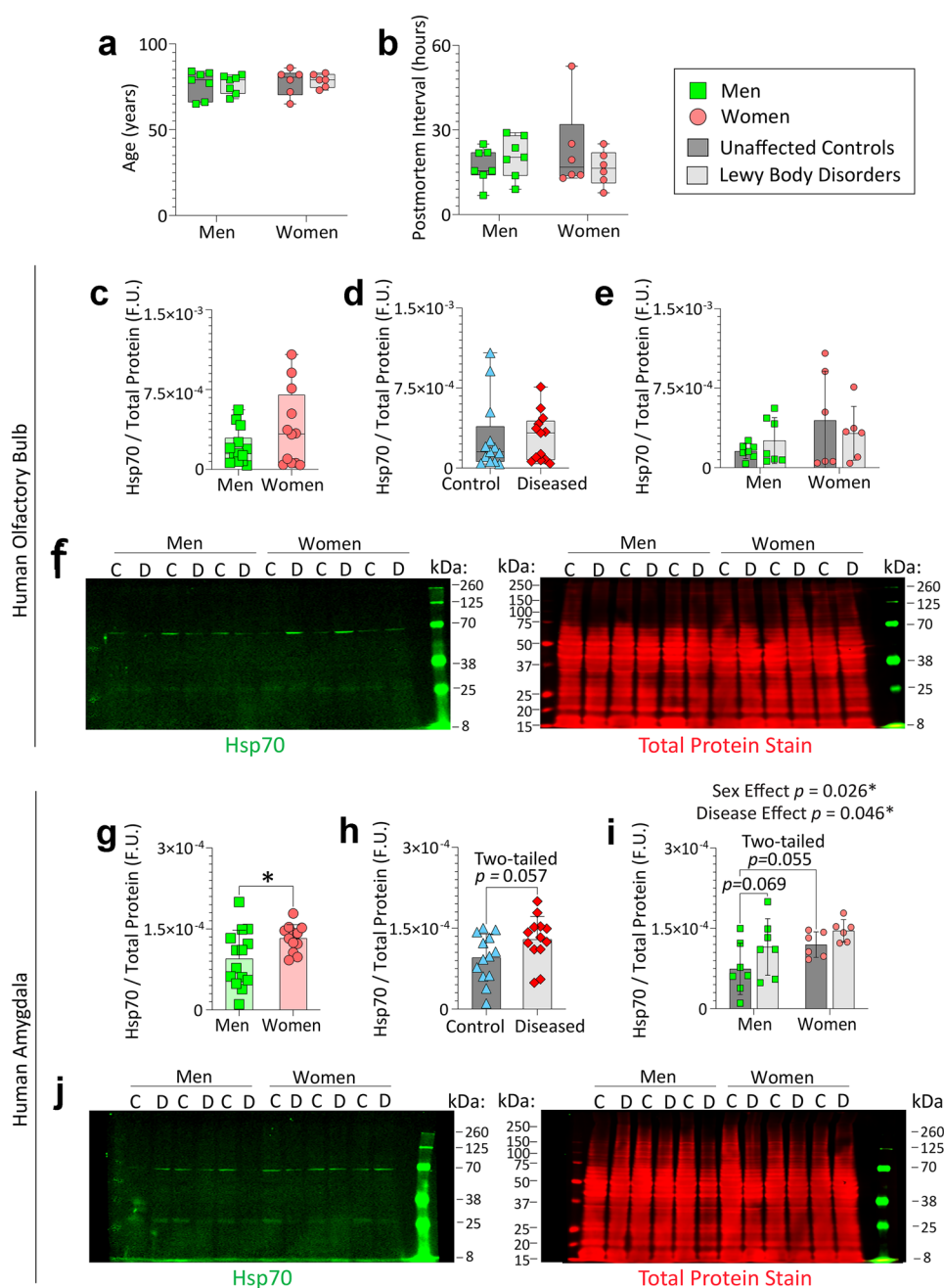
were abolished by pharmacological suppression of Hsp70 chaperone function in male cells. As MAL3-101 inhibits the ability of Hsp40 to activate Hsp70 [81, 104, 108], eHsp70 may be reducing perinuclear inclusion numbers in a manner that depends on Hsp40. (4) Daily intranasal delivery of eHsp70 diminished α-synucleinopathy in aged male mice injected with α-synuclein fibrils in the OB/AON and reduced the latency to contact buried food. Furthermore, delayed but transitory treatment with native eHsp70 enhanced novel arm recognition in the Y-maze, suggestive of long-term improvements in baseline cognitive function. (5) Intranasally infused eHsp70 remained high in the aged male mouse brain up to

24 h and was cleared within 72 h. In addition, aged female brains failed to show evidence of transnasal eHsp70 uptake, although postnatal female primary hippocampal cells displayed eHsp70 uptake in vitro. Further work is needed to determine if females are more likely to degrade eHsp70 within the nasal mucosa or display distinct nose-to-brain barrier properties. (6) Postmortem brain samples collected from women displayed significantly higher Hsp70 expression in the amygdala than samples from age-matched men. Aside from the statistically significant main effects of biological sex in the two-way ANOVA, there were statistically significant main effects of Lewy body disorder diagnoses
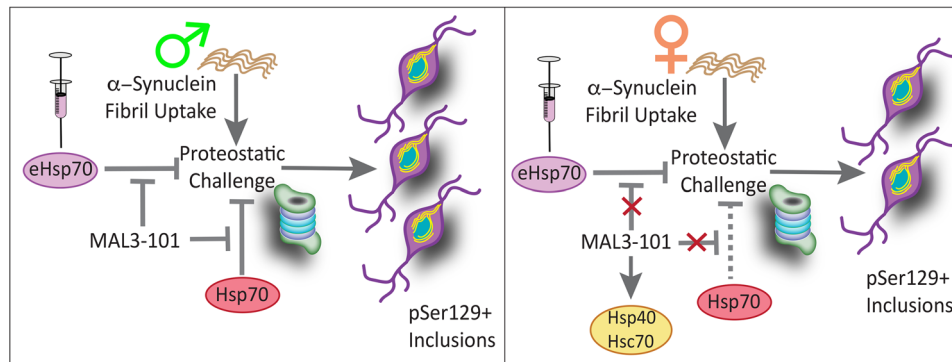
Fig. 9 Summary schematic. Male and female neurons show equivalent uptake of α-synuclein fibrils, but males develop greater nonionic-detergent insoluble α-synucleinopathy than females. Inhibition of endogenous Hsp70 with chaperone-function inhibitor MAL3-101 exacerbated α-synucleinopathy in male cells. Females did not respond as males did to MAL3-101, possibly due to compensatory increases in Hsc70 and Hsp40. Exogenous Hsp70 (eHsp70) reduced α-synucleinopathy in cells of either sex, an effect that was partially dependent on the chaperone function of Hsp70 in male cells

(Fig. 8i) that were largely attributable to men. Collectively, these data support the view that cells in males rely slightly more on Hsp70 expression and function under conditions of proteostatic disequilibria, which may exert cumulative effects over the lifespan.

Strengths and Limitations

A potential limitation is that our study relies on pharmacological means of suppressing Hsp70 function rather than genetic tools or RNA interference. However, the use of the selective inhibitor, MAL3-101, allowed us to test the hypothesis that the Hsp40/ATP-dependent chaperone function of Hsp70 is crucial to temper α-synucleinopathy; MAL3-101 inhibits the Hsp40-mediated increase in Hsp70 ATPase activities, which in turn selectively inhibits Hsp70 chaperone functions [20, 81, 103–106]. In contrast, the less selective VER155008 compound targets the ATP-binding pocket [116], blocking multiple Hsp70 functions (discussed in Crum et al. [109]). It is important to note that, if both inhibitors exert consistent effects, those effects are likely mediated specifically by antagonism of the chaperone activities of Hsp70. It is far less probable that two independent classes of Hsp70 inhibitors would exert the same off-target mechanisms to explain (coincidentally) similar outcomes.

Another caveat of our study is the use of prepubertal rodent cells for modeling age-related Lewy body disorders. Primary neuron cultures from sexually mature adult rodents are problematic to study in vitro for long periods (see Methods). We chose to employ postnatal and not embryonic cultures, so as to divide animals readily by sex as well as increase the anatomical precision of our telencephalic dissections [117]. Aside from neurons, our primary hippocampal cultures harbor 10–13% astroglia: this is perhaps a better reflection of the in vivo milieu than purer neuronal cultures

harvested at embryonic stages prior to massive postnatal gliogenesis. The presence of astroglia might mitigate the neuronal toxicity of preformed fibril exposure (Bhatia and Leak, unpublished), as has also been suggested by others [118]. Nonetheless, it is worth noting that the *HSPA1A* and *HSPA1B* genes are expressed at higher levels in hippocampal neurons compared to astrocytes [119], and ATTO$_{647}$-labeled α-synuclein fibrils are more readily evident within neurons than astrocytes. Indeed, we have not observed pSer129[+] inclusions within cultured astroglia in mixed neural cultures or astrocyte-specific cultures (Bhatia and Leak, unpublished), suggesting that our postnatal hippocampal culture model is appropriate for inducing intense neuronal α-synucleinopathy.

To mitigate potential confounds of studying young cells in vitro, we also examined aged animals at 17–21 months of age. In our work, we rely on both Sprague–Dawley rats and CD-1 mice, partly to avoid fallacious over-standardization of research models and the underappreciated but confounding effects of inbred mouse sub-strains [120, 121]. In contrast, outbred mice (such as CD-1) display higher genetic diversity and are valued for heterogeneity and avoidance of sub-strain confounds [122, 123]. Indeed, findings that generalize across sub-strains and species (e.g., mouse and rat) are more likely to translate to the clinic [120, 121]. Finally, the outbred CD-1 mouse stock ought not to be confused with Jackson's CD1-/- line; the latter has a null mutation in the gene encoding the CD1 antigen complex and thus exhibits natural killer cell deficiency.

In our studies, we did not employ monomeric α-synuclein as a control, because modeling unaffected human control subjects does not, by definition, entail supraphysiologic concentrations of monomeric α-synuclein. Furthermore, it has been reported that monomers can provoke low levels of pSer129[+] pathology [124], as we also observed (Nouraei and

Leak, unpublished). Finally, the use of PBS as a control for eHsp70 avoids the toxicity of potentially aggregated forms of denatured eHsp70; the latter had been included to control for residual endotoxins and other potential substances within the preparation.

We examined Hsp70 levels in whole-tissue extracts, which fails to pinpoint changes within individual cell types. Postmortem intervals from the NeuroBiobank tissues were also relatively long, which may lead to protein degradation, but this caveat is mitigated by the lack of correlation of Hsp70, Hsc70, and Hsp40 levels with postmortem intervals.

Finally, the human subjects analyzed in the present study suffered from various types of Lewy body disorders and were diagnosed at institutions across the USA. On the other hand, we believe that this is a strength rather than a limitation, because results that are statistically significant despite heterogeneity are more likely to generalize across patient cohorts (as argued above for avoiding sub-strains of inbred mice).

Impact of Hsp70 on α-Synucleinopathy

Early studies suggested that Hsp70 does not mitigate pathology in transgenic mice co-overexpressing α-synuclein [125], but forced overexpression could be accompanied by compensatory target downregulation and induction of toxic stress responses. Directed expression of Hsp70 has been reported to reduce dopaminergic neurodegeneration associated with α-synuclein in *Drosophila* [26] and mitigate α-synuclein aggregation in cultured cells, perhaps in cooperation with Hsp40 [126]. The primary culture work reported here expands on prior studies showing that inhibiting Hsp70 activity increases protein aggregation in HEK293T cells overexpressing α-synuclein [95, 126]. Furthermore, in H4 neuroglioma cells transfected with α-synuclein, an allosteric site agonist of the chaperone function of Hsp70 (MAL1-271; aka 115-7c) decreased α-synuclein aggregation [20, 127]. In primary neurons harvested from the olfactory bulb, hippocampus, and cortex, we previously reported that inhibition of endogenous Hsp70 function exacerbates proteotoxic cell loss and raises the levels of ubiquitin-conjugated proteins, a sign of proteostasis failure [97, 109, 128]. In addition, our prior work showed that MAL1-271 reduces proteotoxic cell loss in primary cortical neurons [97].

To our knowledge, the impact of endogenous and exogenous Hsp70 had not previously been tested in primary neurons treated with preformed fibrils as a function of biological sex. Thus, we developed a new sex-stratified model of preformed fibril-induced α-synucleinopathy and discovered that loss of intrinsic Hsp70 function with two inhibitors with distinctly different Hsp70 binding sites encourages greater formation of α-synucleinopathic inclusions in male cells. An alternative interpretation of the data is that pharmacological inhibition of Hsp70 function may hinder the degradation and clearance of inclusions to a greater extent in cells from male mice. Further work is needed to delineate the molecular bases of these effects.

Both MAL3-101 and VER155008 may exert effects on inducible as well as constitutively expressed Hsp70, due to structural similarities in the Hsp70 family of proteins [129]. In primary hippocampal cultures, MAL3-101 raised Hsc70 expression in female cells, a response that could arise from inhibition of either inducible or constitutive Hsp70, or a combination of the two. The rise in expression of the constitutive chaperone Hsc70 (or the co-chaperone Hsp40) during MAL3-101 exposure might allow female cells to suppress an increase in inclusion formation or degrade the inclusions better, and this compensatory response is effectively absent from male cells (schematic in Fig. 9).Thus, male cells may rely more on Hsp70 than female cells to diminish the growth or increase the clearance of pSer129+ inclusions and may be less able to compensate for loss of Hsp70 function.

Based on prior work that eHsp70 enters the brain through the nose and elicits neuroprotective effects in mouse models [53–57, 68], we infused eHsp70 through the nostrils of mice. Nose-to-brain drug delivery would be appropriate for limbic-centered Lewy body disorders, which are sowed in the olfactory system early in the disease [6–8, 28, 73]. We observed that eHsp70 enters the young and aged male CNS after intranasal delivery, but aged female mice did not show evidence of transnasal eHsp70 uptake. In contrast, our in vitro work showed that eHsp70 was taken up by both male and female primary neurons. Potential sex differences in nose-to-brain transit are poorly studied but would be consistent with early work showing lower brain penetration of nasal vesicular stomatitis viral particles in female compared to male mice [130]. Females may also degrade exogenous Hsp70 faster than males, either in the nasal cavity or in the brain itself, perhaps because of the following scenarios: (1) higher numbers of glial cells or more glial reactivity in females than in males [130, 131], (2) higher production of neutralizing peripheral antibodies in females [132], and (3) a more robust immune response upon intranasal infusions of exogenous proteins in females, including an increased infiltration of adaptive immune cells in females and increased expression of molecules such as MHC-II on antigen-presenting cells [130, 132]. Additional work is warranted to tease apart these potential mechanisms.

In aged male mice, we believe that eHsp70 remained active after entry, as it reduced inclusion counts in our proof-of-concept study and also tended to reduce microglial activation. Daily eHsp70 delivery reduced the latency to contact a buried peanut and showed a trend toward a reduced latency to contact the exposed peanut, suggestive perhaps of differences in motivational/hunger status. The strength of the

buried *vs.* exposed food test as performed here is the ability to tease apart differences in motivation rather than olfaction, although recent work suggests that the buried peanut test is not as sensitive as plethysmography of odor-evoked sniffing [133]. For this reason, the odor habituation/dishabituation test was chosen for the long-term neurorescue study. It is also important to note that CD-1 mice have poor vision, especially in old age, and may rely more on smell, even when the food pellet is placed on (and not under) the bedding.

Conclusions

For sake of economy and convenience, cellular and animal models of α-synucleinopathy traditionally focused on mixed sex primary cultures in vitro or young animals of one sex in vivo. Our studies, however, point to the existence of sex differences in the expression and function of endogenous Hsp70 in limbic brain regions and are the first to suggest that male cells may rely more on the function of Hsp70 to combat Lewy-related pathology than female counterparts. In humans, a diagnosis of Lewy body disorders is associated with a statistical trend towards an increase in Hsp70 expression that was largely attributable to men. If these collective findings can be generalized, male patients would be expected to benefit more from therapies targeting Hsp70 function. Future studies are warranted to test potentially sex-dependent pleiotropic functions of eHsp70 (e.g., immunomodulatory, pro-phagocytic, and chaperokine) and the effect of intranasal eHsp70 (perhaps in combination with exogenous Hsp40) on mortality and long-term disease progression in preclinical Lewy body disorders. Finally, this sex-specific work is important in light of the growing number of chaperone modulators being developed [134, 135] and a recent surge in the use of biologics in precision/personalized medicine [136].

References

1. Angot E, Steiner JA, Hansen C, Li JY, Brundin P. Are synucleinopathies prion-like disorders? Lancet Neurol. 2010;9(11):1128-38.
2. Calamini B, Morimoto RI. Protein homeostasis as a therapeutic target for diseases of protein conformation. Curr Top Med Chem. 2012;12(22):2623-40.
3. Jellinger KA. The pathomechanisms underlying Parkinson's disease. Expert Rev Neurother. 2014;14(2):199-215.
4. Fares MB, Jagannath S, Lashuel HA. Reverse engineering Lewy bodies: how far have we come and how far can we go? Nat Rev Neurosci. 2021;22(2):111-31.
5. Breydo L, Wu JW, Uversky VN. Alpha-synuclein misfolding and Parkinson's disease. Biochim Biophys Acta. 2012;1822(2):261-85.
6. Braak H, Del Tredici K, Bratzke H, Hamm-Clement J, Sandmann-Keil D, Rub U. Staging of the intracerebral inclusion body pathology associated with idiopathic Parkinson's disease (preclinical and clinical stages). J Neurol. 2002;249 Suppl 3:III/1–5.
7. Braak H, Del Tredici K, Rub U, de Vos RA, Jansen Steur EN, Braak E. Staging of brain pathology related to sporadic Parkinson's disease. Neurobiol Aging. 2003;24(2):197-211.
8. Braak H, Rub U, Gai WP, Del Tredici K. Idiopathic Parkinson's disease: possible routes by which vulnerable neuronal types may be subject to neuroinvasion by an unknown pathogen. J Neural Transm. 2003;110(5):517-36.
9. Bras IC, Outeiro TF. Alpha-Synuclein: Mechanisms of Release and Pathology Progression in Synucleinopathies. Cells. 2021;10(2).
10. Rodriguez L, Marano MM, Tandon A. Import and Export of Misfolded alpha-Synuclein. Front Neurosci. 2018;12:344.
11. Radons J. The human HSP70 family of chaperones: where do we stand? Cell Stress Chaperones. 2016;21(3):379-404.
12. Evans CG, Chang L, Gestwicki JE. Heat shock protein 70 (hsp70) as an emerging drug target. J Med Chem. 2010;53(12):4585-602.
13. Daugaard M, Rohde M, Jaattela M. The heat shock protein 70 family: Highly homologous proteins with overlapping and distinct functions. FEBS Lett. 2007;581(19):3702-10.
14. Kim YE, Hipp MS, Bracher A, Hayer-Hartl M, Hartl FU. Molecular chaperone functions in protein folding and proteostasis. Annu Rev Biochem. 2013;82:323-55.

15. Ravagnan L, Gurbuxani S, Susin SA, Maisse C, Daugas E, Zamzami N, et al. Heat-shock protein 70 antagonizes apoptosis-inducing factor. Nat Cell Biol. 2001;3(9):839-43.

16. Tao J, Berthet A, Citron YR, Tsiolaki PL, Stanley R, Gestwicki JE, et al. Hsp70 chaperone blocks alpha-synuclein oligomer formation via a novel engagement mechanism. J Biol Chem. 2021:100613.

17. Luk KC, Mills IP, Trojanowski JQ, Lee VM. Interactions between Hsp70 and the hydrophobic core of alpha-synuclein inhibit fibril assembly. Biochemistry. 2008;47(47):12614-25.

18. Aprile FA, Arosio P, Fusco G, Chen SW, Kumita JR, Dhulesia A, et al. Inhibition of alpha-Synuclein Fibril Elongation by Hsp70 Is Governed by a Kinetic Binding Competition between alpha-Synuclein Species. Biochemistry. 2017.

19. Dedmon MM, Christodoulou J, Wilson MR, Dobson CM. Heat shock protein 70 inhibits alpha-synuclein fibril formation via preferential binding to prefibrillar species. J Biol Chem. 2005;280(15):14733-40.

20. Kilpatrick K, Novoa JA, Hancock T, Guerriero CJ, Wipf P, Brodsky JL, et al. Chemical induction of Hsp70 reduces alpha-synuclein aggregation in neuroglioma cells. ACS chemical biology. 2013;8(7):1460-8.

21. Danzer KM, Ruf WP, Putcha P, Joyner D, Hashimoto T, Glabe C, et al. Heat-shock protein 70 modulates toxic extracellular alpha-synuclein oligomers and rescues trans-synaptic toxicity. FASEB J. 2011;25(1):326-36.

22. Klucken J, Shin Y, Masliah E, Hyman BT, McLean PJ. Hsp70 Reduces alpha-Synuclein Aggregation and Toxicity. The Journal of biological chemistry. 2004;279(24):25497-502.

23. Muchowski PJ, Wacker JL. Modulation of neurodegeneration by molecular chaperones. Nature reviews Neuroscience. 2005;6(1):11-22.

24. Kalia SK, Kalia LV, McLean PJ. Molecular chaperones as rational drug targets for Parkinson's disease therapeutics. CNS & neurological disorders drug targets. 2010;9(6):741-53.

25. Wentink AS, Nillegoda NB, Feufel J, Ubartaite G, Schneider CP, De Los Rios P, et al. Molecular dissection of amyloid disaggregation by human HSP70. Nature. 2020;587(7834):483-8.

26. Auluck PK, Chan HY, Trojanowski JQ, Lee VM, Bonini NM. Chaperone suppression of alpha-synuclein toxicity in a Drosophila model for Parkinson's disease. Science. 2002;295(5556):865-8.

27. San Gil R, Cox D, McAlary L, Berg T, Walker AK, Yerbury JJ, et al. Neurodegenerative disease-associated protein aggregates are poor inducers of the heat shock response in neuronal cells. J Cell Sci. 2020;133(15).

28. Beach TG, Adler CH, Lue L, Sue LI, Bachalakuri J, Henry-Watson J, et al. Unified staging system for Lewy body disorders: correlation with nigrostriatal degeneration, cognitive impairment and motor dysfunction. Acta Neuropathol. 2009;117(6):613-34.

29. Nelson PT, Schmitt FA, Jicha GA, Kryscio RJ, Abner EL, Smith CD, et al. Association between male gender and cortical Lewy body pathology in large autopsy series. J Neurol. 2010;257(11):1875-81.

30. Picillo M, Fasano A. How much does sex matter in Parkinson disease? Neurology. 2015;84(21):2102-4.

31. Abraham DS, Gruber-Baldini AL, Magder LS, McArdle PF, Tom SE, Barr E, et al. Sex differences in Parkinson's disease presentation and progression. Parkinsonism Relat Disord. 2019;69:48-54.

32. Larsson V, Torisson G, Londos E. Relative survival in patients with dementia with Lewy bodies and Parkinson's disease dementia. PLoS One. 2018;13(8):e0202044.

33. Cerri S, Mus L, Blandini F. Parkinson's Disease in Women and Men: What's the Difference? J Parkinsons Dis. 2019;9(3):501-15.

34. Williams MM, Xiong C, Morris JC, Galvin JE. Survival and mortality differences between dementia with Lewy bodies vs Alzheimer disease. Neurology. 2006;67(11):1935-41.

35. Haaxma CA, Bloem BR, Borm GF, Oyen WJ, Leenders KL, Eshuis S, et al. Gender differences in Parkinson's disease. J Neurol Neurosurg Psychiatry. 2007;78(8):819-24.

36. Tremblay C, Abbasi N, Zeighami Y, Yau Y, Dadar M, Rahayel S, et al. Sex effects on brain structure in de novo Parkinson's disease: a multimodal neuroimaging study. Brain. 2020.

37. Liu R, Umbach DM, Peddada SD, Xu Z, Troster AI, Huang X, et al. Potential sex differences in nonmotor symptoms in early drug-naive Parkinson disease. Neurology. 2015;84(21):2107-15.

38. Mason DM, Wang Y, Bhatia TN, Miner KM, Trbojevic SA, Stolz JF, et al. The center of olfactory bulb-seeded alpha-synucleinopathy is the limbic system and the ensuing pathology is higher in male than in female mice. Brain Pathol. 2019;29(6):741-70.

39. Pockley AG, Shepherd J, Corton JM. Detection of heat shock protein 70 (Hsp70) and anti-Hsp70 antibodies in the serum of normal individuals. Immunol Invest. 1998;27(6):367-77.

40. Bodega G, Hernandez C, Suarez I, Martin M, Fernandez B. HSP70 constitutive expression in rat central nervous system from postnatal development to maturity. J Histochem Cytochem. 2002;50(9):1161-8.

41. Olazabal UE, Pfaff DW, Mobbs CV. Sex differences in the regulation of heat shock protein 70 kDa and 90 kDa in the rat ventromedial hypothalamus by estrogen. Brain Res. 1992;596(1-2):311-4.

42. Voss MR, Stallone JN, Li M, Cornelussen RN, Knuefermann P, Knowlton AA. Gender differences in the expression of heat shock proteins: the effect of estrogen. Am J Physiol Heart Circ Physiol. 2003;285(2):H687-92.

43. Bundy JL, Vied C, Nowakowski RS. Sex differences in the molecular signature of the developing mouse hippocampus. BMC Genomics. 2017;18(1):237.

44. Schmitt E, Gehrmann M, Brunet M, Multhoff G, Garrido C. Intracellular and extracellular functions of heat shock proteins: repercussions in cancer therapy. J Leukoc Biol. 2007;81(1):15-27.

45. Kono H, Rock KL. How dying cells alert the immune system to danger. Nat Rev Immunol. 2008;8(4):279-89.

46. Bianchi ME. DAMPs, PAMPs and alarmins: all we need to know about danger. J Leukoc Biol. 2007;81(1):1-5.

47. Asea A. Hsp70: a chaperokine. Novartis Found Symp. 2008;291:173–9; discussion 9–83, 221–4.

48. Tytell M. Release of heat shock proteins (Hsps) and the effects of extracellular Hsps on neural cells and tissues. Int J Hyperthermia. 2005;21(5):445-55.

49. Kirkegaard T, Roth AG, Petersen NH, Mahalka AK, Olsen OD, Moilanen I, et al. Hsp70 stabilizes lysosomes and reverts Niemann-Pick disease-associated lysosomal pathology. Nature. 2010;463(7280):549-53.

50. Multhoff G. Heat shock protein 70 (Hsp70): membrane location, export and immunological relevance. Methods. 2007;43(3):229-37.

51. Calderwood SK, Mambula SS, Gray PJ, Jr., Theriault JR. Extracellular heat shock proteins in cell signaling. FEBS Lett. 2007;581(19):3689-94.

52. Dukay B, Csoboz B, Toth ME. Heat-Shock Proteins in Neuroinflammation. Front Pharmacol. 2019;10:920.

53. Bobkova NV, Evgen'ev M, Garbuz DG, Kulikov AM, Morozov A, Samokhin A, et al. Exogenous Hsp70 delays senescence and improves cognitive function in aging mice. Proc Natl Acad Sci U S A. 2015;112(52):16006-11.

54. Bobkova NV, Garbuz DG, Nesterova I, Medvinskaya N, Samokhin A, Alexandrova I, et al. Therapeutic effect of exogenous hsp70 in mouse models of Alzheimer's disease. J Alzheimers Dis. 2014;38(2):425-35.

55. Tytell M, Davis AT, Giles J, Snider LC, Xiao R, Dozier SG, et al. Alfalfa-derived HSP70 administered intranasally improves insulin sensitivity in mice. Cell Stress Chaperones. 2018;23(2):189-94.

56. Demyanenko S, Nikul V, Rodkin S, Davletshin A, Evgen'ev MB, Garbuz DG. Exogenous recombinant Hsp70 mediates neuroprotection after photothrombotic stroke. Cell Stress Chaperones. 2021;26(1):103-14.

57. Evgen'ev M, Bobkova N, Krasnov G, Garbuz D, Funikov S, Kudryavtseva A, et al. The Effect of Human HSP70 Administration on a Mouse Model of Alzheimer's Disease Strongly Depends on Transgenicity and Age. J Alzheimers Dis. 2019;67(4):1391-404.

58. Hanson LR, Frey WH, 2nd. Intranasal delivery bypasses the blood-brain barrier to target therapeutic agents to the central nervous system and treat neurodegenerative disease. BMC Neurosci. 2008;9 Suppl 3:S5.

59. Thorne RG, Pronk GJ, Padmanabhan V, Frey WH, 2nd. Delivery of insulin-like growth factor-I to the rat brain and spinal cord along olfactory and trigeminal pathways following intranasal administration. Neuroscience. 2004;127(2):481-96.

60. Kozlovskaya L, Abou-Kaud M, Stepensky D. Quantitative analysis of drug delivery to the brain via nasal route. J Control Release. 2014;189C:133-40.

61. Arnold TH, Tackett RL, Vallner JJ. Pharmacodynamics of acute intranasal administration of verapamil: comparison with i.v. and oral administration. Biopharm Drug Dispos. 1985;6(4):447–54.

62. Wen MM. Olfactory targeting through intranasal delivery of biopharmaceutical drugs to the brain: current development. Discov Med. 2011;11(61):497-503.

63. Meredith ME, Salameh TS, Banks WA. Intranasal Delivery of Proteins and Peptides in the Treatment of Neurodegenerative Diseases. AAPS J. 2015;17(4):780-7.

64. Dhuria SV, Hanson LR, Frey WH, 2nd. Intranasal delivery to the central nervous system: mechanisms and experimental considerations. J Pharm Sci. 2010;99(4):1654-73.

65. Theriault JR, Adachi H, Calderwood SK. Role of scavenger receptors in the binding and internalization of heat shock protein 70. J Immunol. 2006;177(12):8604-11.

66. Anand PK, Anand E, Bleck CK, Anes E, Griffiths G. Exosomal Hsp70 induces a pro-inflammatory response to foreign particles including mycobacteria. PLoS One. 2010;5(4):e10136.

67. Evgen'ev MB, Krasnov GS, Nesterova IV, Garbuz DG, Karpov VL, Morozov AV, et al. Molecular Mechanisms Underlying Neuroprotective Effect of Intranasal Administration of Human Hsp70 in Mouse Model of Alzheimer's Disease. J Alzheimers Dis. 2017;59(4):1415-26.

68. Pastukhov YF, Plaksina DV, Lapshina KV, Guzhova IV, Ekimova IV. Exogenous protein HSP70 blocks neurodegeneration in the rat model of the clinical stage of Parkinson's disease. Dokl Biol Sci. 2014;457(1):225-7.

69. Tiefensee Ribeiro C, Peixoto DO, Santos L, Saibro-Girardi C, Brum PO, Carazza-Kessler FG, et al. Intranasal HSP70 administration protects against dopaminergic denervation and modulates neuroinflammatory response in the 6-OHDA rat model. Brain, Behavior, & Immunity - Health. 2021;14:100253.

70. Attems J, Walker L, Jellinger KA. Olfactory bulb involvement in neurodegenerative diseases. Acta neuropathologica. 2014;127(4):459-75.

71. Daniel SE, Hawkes CH. Preliminary diagnosis of Parkinson's disease by olfactory bulb pathology. Lancet. 1992;340(8812):186.

72. Adler CH, Beach TG. Neuropathological basis of nonmotor manifestations of Parkinson's disease. Mov Disord. 2016;31(8):1114-9.

73. Beach TG, White CL, 3rd, Hladik CL, Sabbagh MN, Connor DJ, Shill HA, et al. Olfactory bulb alpha-synucleinopathy has high specificity and sensitivity for Lewy body disorders. Acta Neuropathol. 2009;117(2):169-74.

74. Volpicelli-Daley LA, Luk KC, Lee VM. Addition of exogenous alpha-synuclein preformed fibrils to primary neuronal cultures to seed recruitment of endogenous alpha-synuclein to Lewy body and Lewy neurite-like aggregates. Nat Protoc. 2014;9(9):2135-46.

75. Luk KC, Kehm V, Carroll J, Zhang B, O'Brien P, Trojanowski JQ, et al. Pathological alpha-synuclein transmission initiates Parkinson-like neurodegeneration in nontransgenic mice. Science. 2012;338(6109):949-53.

76. Luk KC, Kehm VM, Zhang B, O'Brien P, Trojanowski JQ, Lee VM. Intracerebral inoculation of pathological alpha-synuclein initiates a rapidly progressive neurodegenerative alpha-synucleinopathy in mice. J Exp Med. 2012;209(5):975-86.

77. Luk KC, Song C, O'Brien P, Stieber A, Branch JR, Brunden KR, et al. Exogenous alpha-synuclein fibrils seed the formation of Lewy body-like intracellular inclusions in cultured cells. Proc Natl Acad Sci U S A. 2009;106(47):20051-6.

78. Volpicelli-Daley LA, Luk KC, Patel TP, Tanik SA, Riddle DM, Stieber A, et al. Exogenous alpha-synuclein fibrils induce Lewy body pathology leading to synaptic dysfunction and neuron death. Neuron. 2011;72(1):57-71.

79. Mason DM, Nouraei N, Pant DB, Miner KM, Hutchison DF, Luk KC, et al. Transmission of alpha-synucleinopathy from olfactory structures deep into the temporal lobe. Mol Neurodegener. 2016;11(1):49.

80. Nouraei N, Mason DM, Miner KM, Carcella MA, Bhatia TN, Dumm BK, et al. Critical appraisal of pathology transmission in the alpha-synuclein fibril model of Lewy body disorders. Exp Neurol. 2018;299(Pt A):172-96.

81. Fewell SW, Smith CM, Lyon MA, Dumitrescu TP, Wipf P, Day BW, et al. Small molecule modulators of endogenous and cochaperone-stimulated Hsp70 ATPase activity. The Journal of biological chemistry. 2004;279(49):51131-40.

82. Ireland AW, Gobillot TA, Gupta T, Seguin SP, Liang M, Resnick L, et al. Synthesis and structure-activity relationships of small molecule inhibitors of the simian virus 40 T antigen oncoprotein, an anti-polyomaviral target. Bioorg Med Chem. 2014;22(22):6490-502.

83. McClellan AJ, Brodsky JL. Mutation of the ATP-binding pocket of SSA1 indicates that a functional interaction between Ssa1p and Ydj1p is required for post-translational translocation into the yeast endoplasmic reticulum. Genetics. 2000;156(2):501-12.

84. Paxinos G, Franklin KBJ. Paxinos and Franklin's The mouse brain in stereotaxic coordinates. Fourth edition. ed. Amsterdam: Academic Press, an imprint of Elsevier; 2013. 1 volume (unpaged)

85. Fleming SM, Tetreault NA, Mulligan CK, Hutson CB, Masliah E, Chesselet MF. Olfactory deficits in mice overexpressing human wildtype alpha-synuclein. Eur J Neurosci. 2008;28(2):247-56.

86. Lehmkuhl AM, Dirr ER, Fleming SM. Olfactory assays for mouse models of neurodegenerative disease. J Vis Exp. 2014;(90):e51804.

87. Rey NL, Steiner JA, Maroof N, Luk KC, Madaj Z, Trojanowski JQ, et al. Widespread transneuronal propagation of alpha-synucleinopathy triggered in olfactory bulb mimics prodromal Parkinson's disease. J Exp Med. 2016;213(9):1759-78.

88. Wolf A, Bauer B, Abner EL, Ashkenazy-Frolinger T, Hartz AM. A Comprehensive Behavioral Test Battery to Assess Learning and Memory in 129S6/Tg2576 Mice. PLoS One. 2016;11(1):e0147733.

89. Frye CA, Petralia SM, Rhodes ME. Estrous cycle and sex differences in performance on anxiety tasks coincide with increases in hippocampal progesterone and 3alpha,5alpha-THP. Pharmacol Biochem Behav. 2000;67(3):587-96.

90. Seibenhener ML, Wooten MC. Use of the Open Field Maze to measure locomotor and anxiety-like behavior in mice. J Vis Exp. 2015(96):e52434.

91. Luna E, Decker SC, Riddle DM, Caputo A, Zhang B, Cole T, et al. Differential alpha-synuclein expression contributes to selective vulnerability of hippocampal neuron subpopulations to fibril-induced toxicity. Acta Neuropathol. 2018;135(6):855-75.

92. Courte J, Bousset L, Boxberg YV, Villard C, Melki R, Peyrin JM. The expression level of alpha-synuclein in different neuronal populations is the primary determinant of its prion-like seeding. Sci Rep. 2020;10(1):4895.

93. Mahul-Mellier AL, Burtscher J, Maharjan N, Weerens L, Croisier M, Kuttler F, et al. The process of Lewy body formation, rather than simply alpha-synuclein fibrillization, is one of the major drivers of neurodegeneration. Proc Natl Acad Sci U S A. 2020;117(9):4971-82.

94. Schaser AJ, Stackhouse TL, Weston LJ, Kerstein PC, Osterberg VR, Lopez CS, et al. Trans-synaptic and retrograde axonal spread of Lewy pathology following pre-formed fibril injection in an in vivo A53T alpha-synuclein mouse model of synucleinopathy. Acta Neuropathol Commun. 2020;8(1):150.

95. McLean PJ, Kawamata H, Shariff S, Hewett J, Sharma N, Ueda K, et al. TorsinA and heat shock proteins act as molecular chaperones: suppression of alpha-synuclein aggregation. Journal of neurochemistry. 2002;83(4):846-54.

96. Robinson MB, Tidwell JL, Gould T, Taylor AR, Newbern JM, Graves J, et al. Extracellular heat shock protein 70: a critical component for motoneuron survival. J Neurosci. 2005;25(42):9735-45.

97. Posimo JM, Weilnau JN, Gleixner AM, Broeren MT, Weiland NL, Brodsky JL, et al. Heat shock protein defenses in the neocortex and allocortex of the telencephalon. Neurobiol Aging. 2015;36(5):1924-37.

98. Volpicelli-Daley LA, Gamble KL, Schultheiss CE, Riddle DM, West AB, Lee VM. Formation of alpha-synuclein Lewy neurite-like aggregates in axons impedes the transport of distinct endosomes. Mol Biol Cell. 2014;25(25):4010-23.

99. Kumar ST, Jagannath S, Francois C, Vanderstichele H, Stoops E, Lashuel HA. How specific are the conformation-specific alpha-synuclein antibodies? Characterization and validation of 16 alpha-synuclein conformation-specific antibodies using well-characterized preparations of alpha-synuclein monomers, fibrils and oligomers with distinct structures and morphology. Neurobiol Dis. 2020;146:105086.

100. Hocquemiller M, Vitry S, Bigou S, Bruyere J, Ausseil J, Heard JM. GAP43 overexpression and enhanced neurite outgrowth in mucopolysaccharidosis type IIIB cortical neuron cultures. J Neurosci Res. 2010;88(1):202-13.

101. Bigler RL, Kamande JW, Dumitru R, Niedringhaus M, Taylor AM. Messenger RNAs localized to distal projections of human stem cell derived neurons. Sci Rep. 2017;7(1):611.

102. Williamson DS, Borgognoni J, Clay A, Daniels Z, Dokurno P, Drysdale MJ, et al. Novel adenosine-derived inhibitors of 70 kDa heat shock protein, discovered through structure-based design. Journal of medicinal chemistry. 2009;52(6):1510-3.

103. Huryn DM, Brodsky JL, Brummond KM, Chambers PG, Eyer B, Ireland AW, et al. Chemical methodology as a source of small-molecule checkpoint inhibitors and heat shock protein 70 (Hsp70) modulators. Proceedings of the National Academy of Sciences of the United States of America. 2011;108(17):6757-62.

104. Braunstein MJ, Scott SS, Scott CM, Behrman S, Walter P, Wipf P, et al. Antimyeloma Effects of the Heat Shock Protein 70 Molecular Chaperone Inhibitor MAL3–101. Journal of oncology. 2011;2011:232037.

105. Hatic H, Kane MJ, Saykally JN, Citron BA. Modulation of transcription factor Nrf2 in an in vitro model of traumatic brain injury. Journal of neurotrauma. 2012;29(6):1188-96.

106. Adam C, Baeurle A, Brodsky JL, Wipf P, Schrama D, Becker JC, et al. The HSP70 Modulator MAL3–101 Inhibits Merkel Cell Carcinoma. PLoS One. 2014;9(4):e92041.

107. Flaherty KM, DeLuca-Flaherty C, McKay DB. Three-dimensional structure of the ATPase fragment of a 70K heat-shock cognate protein. Nature. 1990;346(6285):623-8.

108. Fan CY, Lee S, Cyr DM. Mechanisms for regulation of Hsp70 function by Hsp40. Cell Stress Chaperones. 2003;8(4):309-16.

109. Crum TS, Gleixner AM, Posimo JM, Mason DM, Broeren MT, Heinemann SD, et al. Heat shock protein responses to aging and proteotoxicity in the olfactory bulb. J Neurochem. 2015;133(6):780-94.

110. Rey NL, George S, Steiner JA, Madaj Z, Luk KC, Trojanowski JQ, et al. Spread of aggregates after olfactory bulb injection of alpha-synuclein fibrils is associated with early neuronal loss and is reduced long term. Acta Neuropathol. 2018;135(1):65-83.

111. Rey NL, Steiner JA, Maroof N, Luk KC, Madaj Z, Trojanowski JQ, et al. Widespread transneuronal propagation of alpha-synucleinopathy triggered in olfactory bulb mimics prodromal Parkinson's disease. J Exp Med. 2016.

112. Rey NL, Wesson DW, Brundin P. The olfactory bulb as the entry site for prion-like propagation in neurodegenerative diseases. Neurobiol Dis. 2016.

113. Uemura N, Ueda J, Yoshihara T, Ikuno M, Uemura MT, Yamakado H, et al. alpha-Synuclein Spread from Olfactory Bulb Causes Hyposmia, Anxiety, and Memory Loss in BAC-SNCA Mice. Mov Disord. 2021.

114. Uemura N, Uemura MT, Lo A, Bassil F, Zhang B, Luk KC, et al. Slow Progressive Accumulation of Oligodendroglial Alpha-Synuclein (alpha-Syn) Pathology in Synthetic alpha-Syn Fibril-Induced Mouse Models of Synucleinopathy. J Neuropathol Exp Neurol. 2019;78(10):877-90.

115. Kushnirov VV, Kryndushkin DS, Boguta M, Smirnov VN, Ter-Avanesyan MD. Chaperones that cure yeast artificial [PSI+] and their prion-specific effects. Curr Biol. 2000;10(22):1443-6.

116. Schlecht R, Scholz SR, Dahmen H, Wegener A, Sirrenberg C, Musil D, et al. Functional analysis of Hsp70 inhibitors. PLoS One. 2013;8(11):e78443.

117. Posimo JM, Titler AM, Choi HJ, Unnithan AS, Leak RK. Neocortex and allocortex respond differentially to cellular stress in vitro and aging in vivo. PLoS One. 2013;8(3):e58596.

118. Loria F, Vargas JY, Bousset L, Syan S, Salles A, Melki R, et al. alpha-Synuclein transfer between neurons and astrocytes indicates that astrocytes play a role in degradation rather than in spreading. Acta Neuropathol. 2017;134(5):789-808.

119. Saunders A, Macosko EZ, Wysoker A, Goldman M, Krienen FM, de Rivera H, et al. Molecular Diversity and Specializations among the Cells of the Adult Mouse Brain. Cell. 2018;174(4):1015–30 e16.

120. Voelkl B, Vogt L, Sena ES, Wurbel H. Reproducibility of preclinical animal research improves with heterogeneity of study samples. PLoS Biol. 2018;16(2):e2003693.

121. Wurbel H. Behaviour and the standardization fallacy. Nat Genet. 2000;26(3):263.

122. Aldinger KA, Sokoloff G, Rosenberg DM, Palmer AA, Millen KJ. Genetic variation and population substructure in outbred CD-1 mice: implications for genome-wide association studies. PLoS One. 2009;4(3):e4729.

123. Hsieh LS, Wen JH, Miyares L, Lombroso PJ, Bordey A. Outbred CD1 mice are as suitable as inbred C57BL/6J mice in performing social tasks. Neurosci Lett. 2017;637:142-7.

124. Paumier KL, Luk KC, Manfredsson FP, Kanaan NM, Lipton JW, Collier TJ, et al. Intrastriatal injection of pre-formed mouse alpha-synuclein fibrils into rats triggers alpha-synuclein pathology and bilateral nigrostriatal degeneration. Neurobiol Dis. 2015;82:185-99.

125. Shimshek DR, Mueller M, Wiessner C, Schweizer T, van der Putten PH. The HSP70 molecular chaperone is not beneficial in a mouse model of alpha-synucleinopathy. PLoS One. 2010;5(4):e10014.

126. Aprile FA, Kallstig E, Limorenko G, Vendruscolo M, Ron D, Hansen C. The molecular chaperones DNAJB6 and Hsp70 cooperate to suppress alpha-synuclein aggregation. Sci Rep. 2017;7(1):9039.

127. Chiang AN, Liang M, Dominguez-Meijide A, Masaracchia C, Goeckeler-Fried JL, Mazzone CS, et al. Synthesis and evaluation of esterified Hsp70 agonists in cellular models of protein aggregation and folding. Bioorg Med Chem. 2019;27(1):79-91.

128. Heinemann SD, Posimo JM, Mason DM, Hutchison DF, Leak RK. Synergistic stress exacerbation in hippocampal neurons: Evidence favoring the dual-hit hypothesis of neurodegeneration. Hippocampus. 2016;26(8):980-94.

129. Mayer MP, Bukau B. Hsp70 chaperones: cellular functions and molecular mechanism. Cellular and molecular life sciences : CMLS. 2005;62(6):670-84.

130. Barna M, Komatsu T, Bi Z, Reiss CS. Sex differences in susceptibility to viral infection of the central nervous system. J Neuroimmunol. 1996;67(1):31-9.

131. Oliveira-Pinto AV, Santos RM, Coutinho RA, Oliveira LM, Santos GB, Alho AT, et al. Sexual dimorphism in the human olfactory bulb: females have more neurons and glial cells than males. PLoS One. 2014;9(11):e111733.

132. Fink AL, Engle K, Ursin RL, Tang WY, Klein SL. Biological sex affects vaccine efficacy and protection against influenza in mice. Proc Natl Acad Sci U S A. 2018;115(49):12477-82.

133. Johnson ME, Bergkvist L, Mercado G, Stetzik L, Meyerdirk L, Wolfrum E, et al. Deficits in olfactory sensitivity in a mouse model of Parkinson's disease revealed by plethysmography of odor-evoked sniffing. Sci Rep. 2020;10(1):9242.

134. Chaudhury S, Keegan BM, Blagg BSJ. The role and therapeutic potential of Hsp90, Hsp70, and smaller heat shock proteins in peripheral and central neuropathies. Med Res Rev. 2020.

135. Ebrahimi-Fakhari D, Saidi LJ, Wahlster L. Molecular chaperones and protein folding as therapeutic targets in Parkinson's disease and other synucleinopathies. Acta Neuropathol Commun. 2013;1:79.

136. Kinch MS. An overview of FDA-approved biologics medicines. Drug Discov Today. 2015;20(4):393-8.

Publisher's Note Springer Nature remains neutral with regard to jurisdictional claims in published maps and institutional affiliations.